## CRITICAL REVIEW

Check for updates

# Aptamer selection *via* versatile microfluidic platforms and their diverse applications

Yi-Da Chung,[a] Yi-Cheng Tsai,[a] Chi-Hung Wang[a] and Gwo-Bin Lee ![ORCID] *[abc]

Aptamers are synthetic oligonucleotides that bind with high affinity and specificity to various targets, making them invaluable for diagnostics, therapeutics, and biosensing. Microfluidic platforms can improve the efficiency and scalability of aptamer selection, especially through advancements in systematic evolution of ligands by exponential enrichment (SELEX) methods. Microfluidic SELEX methods are less time-consuming and labor-intensive and include critical steps like library preparation, binding, partitioning, and amplification. This review examines the contributions of microfluidic technology to SELEX-based aptamer identification, with alternative methods like conditional SELEX, *in vivo*-like SELEX and Non-SELEX for selecting aptamers and also discusses critical SELEX steps over the past decade. This work also examined the integrated microfluidic systems for SELEX, highlighting innovations such as conditional SELEX and *in vivo*-like SELEX. These advancements provide potential solutions to existing challenges in aptamer selection using conventional SELEX, especially concerning biological samples. A trend toward non-SELEX methods was also reviewed and discussed, wherein nucleic acid amplification was eliminated to improve aptamer selection. Microfluidic platforms have demonstrated versatility not only in aptamer selection but also in various detection applications; they allow for precise control of liquid flow and have been essential in the advancement of therapeutic aptamers, facilitating accurate screening, enhancing drug delivery systems, and enabling targeted therapeutic interventions. Although advances in microfluidic technology are expected to enhance aptamer-based diagnostics, therapeutics, and biosensing, challenges still persist, especially in up-scaling microfluidic systems for various clinical applications. The advantages and limitations of integrating microfluidic platforms with aptamer development are further addressed, emphasizing areas for future research. We also present a perspective on the future of microfluidic systems and aptamer technologies, highlighting their increasing significance in healthcare and diagnostics.

## 1. Introduction

Aptamers are short, single-stranded DNA or RNA molecules that can bind to a diverse range of targets, including small molecules (such as toxins & antibiotics), proteins, and even cells/tissues, with high specificity and affinity.[1–4] This versatility stems from their ability to fold into unique three-dimensional (3D) structures, enabling them to interact with their targets in a highly specific manner (akin to antibody–antigen interactions[5,6]). The exceptional target-binding capabilities of aptamers have garnered significant scientific and biological interest, opening up applications in fields such as molecular diagnostics, therapeutics, and biosensing.[7,8] Aptamers offer several advantages over traditional antibodies. They are far smaller in size (only 25–80 base-pairs (bp)), allowing for improved tissue penetration and pharmacokinetics.[9–11] Unlike conventional antibodies, they lack immunogenicity, reducing the risk of adverse reactions,[12] and they can withstand changes in temperature and humidity.[13–15] Aptamers can be produced through cost-effective chemical synthesis at 100% accuracy, in contrast to the significant batch-to-batch variation caused by the complex animal-based production of antibodies.[16,17] These advantages, alongside their versatility,[18–20] have driven extensive research on the development of efficient aptamer selection methods for diverse applications over recent decades.[4,21–23]

The screening or selection of aptamers begins with a large pool of random nucleic acids ($10^{12}$ to $10^{15}$ unique single-stranded DNAs (ssDNAs)) that is systematically screened to identify high-affinity and high-specificity probes to the target of interest.[22,24] The "systematic evolution of ligands by exponential enrichment" (SELEX) process, originally developed in the 1990s, is the versatile and robust cornerstone of aptamer selection[25,26]

*[a] Department of Power Mechanical Engineering, National Tsing Hua University, Hsinchu, Taiwan. E-mail: gwobin@pme.nthu.edu.tw;*
*Tel: +886 3 5715131 Ext. 33765*
*[b] Institute of NanoEngineering and MicroSystems, National Tsing Hua University, Hsinchu, Taiwan*
*[c] Institute of Biomedical Engineering, National Tsing Hua University, Hsinchu, Taiwan*

and involves binding, separation, and amplification (*via* polymerase chain reaction (PCR)) of screened ssDNA with the desired characteristics.[5,20] However, SELEX suffers from lengthy, inefficient ssDNA library+target molecules incubations and ssDNA amplification processes. Moreover, incomplete removal of unbound or weakly-bound ssDNA, which may be amplified by the subsequent PCR and can compete with better candidates in subsequent screening rounds, are also critical issues. Moreover, the total number of the screening rounds may be at least 10–20, which may take weeks or months, and post-SELEX processes that require modification of screened aptamers can compromise aptamer integrity.

Microfluidic technology, which emerged in the late 1980s, is a multidisciplinary field that combines engineering, physics, chemistry, and biology.[27–30] It enables precise manipulation and control of small fluid volumes (at nL–pL scale) within microchannels or other microfabricated devices (*e.g.*, micropumps, micromixers, & microvalves).[31–33] The advantages of microfluidics, namely precise control over flow rate, volume, and incubation time, have enabled the development of highly efficient and sensitive analytical screening platforms.[34–36] The integration of microfluidic technology with aptamer selection methods, known as "microfluidic SELEX", has revolutionized the field of aptamer

**Yi-Da Chung**

*Yi-Da Chung received his M.S. degree from the Department of Life Sciences at National Tsing Hua University, Taiwan, in 1998. Currently, he is a PhD candidate in the Department of Power Mechanical Engineering at National Tsing Hua University, Taiwan. His research expertise includes the technology of aptamer selection, SELEX, and the development of microfluidic chips and biosensors.*



**Yi-Cheng Tsai**

*Yi-Cheng Tsai received his BS and MS degrees from the Department of life science and the Institute of Biomedical sciences at Chang Gung University, Taiwan in 2007 and 2009, respectively. He completed his PhD study at the Graduate Institute of Biomedical Science, Division of Biochemistry, Molecular and Cellular Biology of Chang Gung University, Taiwan in 2014. Currently, he is a post-doctoral fellow in the Department of Power Mechanical Engineering at National Tsing Hua University, Taiwan. His research specialties are molecular biology, molecular diagnosis and nanobiotechnology.*



**Chih-Hung Wang**

*Chih-Hung Wang received his B. S. and M.S. He obtained degrees from the Department of Plant Pathology and the Institute of Molecular Biology at National Chung Hsing University, Taiwan in 1989 and 1994, respectively. He completed his Ph.D. studies at the Institute of Basic Medical Science of National Cheng Kung University, Taiwan in 2005. He has worked at AsiaGen Corporation, exploring molecular diagnosis technologies. Currently, he is a postdoctoral fellow in the Department of Power Mechanical Engineering at National Tsing Hua University, Taiwan. His research specialties are molecular diagnosis, microbiology, and nanobiotechnology*



**Gwo-Bin Lee**

*Gwo-Bin Lee received his BS and MS degrees from the Department of Mechanical Engineering at National Taiwan University in 1989 and 1991, respectively. He received his PhD from the Department of Mechanical & Aerospace Engineering at the University of California, Los Angeles, USA in 1998. He is a Tsing Hua Chair Professor in the Department of Power Mechanical Engineering at National Tsing Hua University, Taiwan. His research interests are on microfluidics, bio-sensing, nanobiotechnology and its biomedical applications. He was an elected Fellow of NAI, ASME, RSC, IET, IEEE, AIMBE. He is a Member of European Academy of Sciences and Arts and a member of International Institute of Engineering. He is Editor-in-chief of Microfluidics and Nanofluidics. He is the recipient of the prestigious IEEE EDS Robert Bosch Micro and Nano Electro Mechanical Systems Award 2025.*

development.[37–43] These microfluidic features have also facilitated the lab-on-a-chip concept, integrating multiple laboratory functions onto a single, compact, automated device.[44] Microfluidic SELEX offers advantages like reduced sample/reagent volume, improved target-binding capacity, enhanced selection stringency, and automated/parallel processing for improved throughput.[45] These advantages have led to various microfluidic-based SELEX techniques that further improve efficiency and speed of aptamer screening.[46–49] Originally, SELEX was used to select aptamers targeting proteins, eventually expanded to other targets like cells (cell-SELEX[50–53]) or tissues.[39,54] Other variations include capillary electrophoresis SELEX (CE-SELEX),[55–57] capture-SELEX,[58,59] magnetic bead (MB)-SELEX,[60–62] and many others.[63–66] Notably, there are also methods like non-SELEX,[67] or hydrogel for aptamer selection (HAS) method,[68] applying other biomaterials and alternative platforms for overcoming amplification bias or non-specific binding issues to improve the efficiency on aptamer selection. Moreover, small molecules up to complex biological entities can be probed with aptamers screened through these methods.[54,66] These targets and approaches have been demonstrated in microfluidic platforms in the past decades.

Previous reviews have highlighted the integration of microfluidic technology with SELEX,[5,24,45,67,69–71] as well as the potential of aptamers to be used in diagnostic and therapeutic applications. Herein we focus instead on advancements in microfluidic SELEX and subsequent aptamer applications over the past 10 years. We first discuss how microfluidic technology has enhanced key steps of the SELEX process. Secondly, we review the diverse applications of aptamers enabled by microfluidic technology over the last five years. Finally, we discuss major challenges with, and a future prospective of, these technologies.

## 2. Microfluidic platforms and aptamer selection methodologies

### 2.1 The SELEX method

SELEX involves an iterative process of 1) binding a random oligonucleotide library to the target, 2) separating the bound sequences, and 3) amplifying them with PCR. This process gradually enriches the library with high-affinity and high-specificity probes as follows (Fig. 1).

1. Library preparation: generating a diverse pool of ssDNAs/RNA oligonucleotides.

2. Binding: incubating and mixing the oligonucleotide library with the target analytes.

3. Partition: separating bound from unbound oligonucleotides.

4. Elution and amplification: enrichment of the high-affinity aptamers.

5. Cloning, sequencing/synthesis, and characterization: analyzing the sequences of the aptamer candidates, followed by modeling/measuring their binding characteristics.

Miniaturized microfluidic platforms enhance the efficiency of aptamer selection by automating labor-intensive, time-consuming processes. When compared to conventional methods, microfluidic approaches are faster, require considerably less precious samples and expensive reagents, and can be automated with less human intervention. Furthermore, they allow for more precise control of reaction/washing conditions (*e.g.*, pH, temperature, & shearing forces) such that more efficient screening for high-affinity and highly specific aptamers can be performed. Aptamer probes targeting proteins, viruses, bacteria, cancer cells, and even cancer tissue biomarkers are now available and will likely replace conventional antibodies.
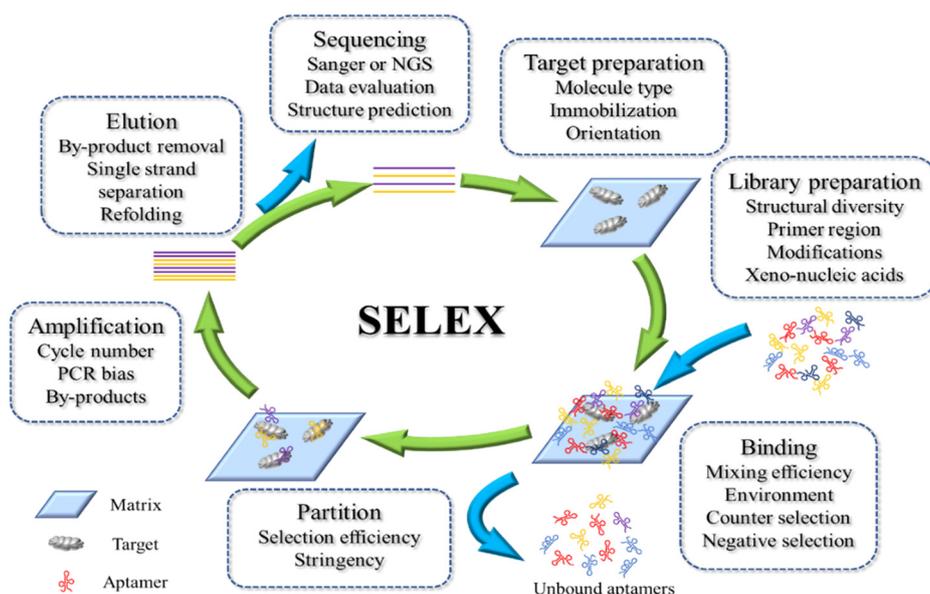


Fig. 1 Schematic view of conventional SELEX with critical steps. Several important issues of each step are also listed.

## 2.2 Library preparation

The diversity of the initial oligonucleotide library is crucial for the success of aptamer selection. Aptamer libraries normally consist of random, unique DNA or RNA sequences ($n = 10^{12}$ to $10^{15}$) flanked by fixed primer-binding sites. Such a large number of potential probes better ensures that at least some bind to the target of interest. The screened pool from each selection round then serves as the library for the subsequent one. Thus, preparing a high-quality candidate pool is critical. Although some original SELEX protocols used random RNAs,[25,26] most SELEX libraries in use today are DNA-based, as DNA oligonucleotides are more stable and easier to synthesize.[72,73] Generally speaking, microfluidic technologies do not play a role in library preparation, though several intriguing exceptions are highlighted below and more detail information are listed in Table 1.

### 2.2.1 Screening for xeno-nucleic acid polymerases.
Synthetic nucleic acids, such as xeno-nucleic acids (XNA), have garnered attention due to their unique properties.[106] One type, α-L-threofuranosyl nucleic acid (TNA), exhibits not only high stability but also the ability to form base pairs with DNA/RNA.[74] A droplet-based optical polymerase sorting (DrOPS) method was developed to evolve polymerases capable of synthesizing TNA. DrOPS involves 1) encapsulating *E. coli* cells expressing polymerase variants in microfluidic droplets, 2) lysing the cells, and 3) sorting the droplets based on activity of the polymerases.[75,76] Using DrOPS, researchers evolved a highly efficient TNA polymerase: Kod-RSGA.[77] The DrOPS method has proven valuable for engineering polymerases that can synthesize diverse XNAs. The DrOPS method was not directly used for library preparation but could enhance polymerase evolution, expanding the diversity of nucleic acid candidates for SELEX and enabling new possibilities in synthetic genetics and biotechnology.

### 2.2.2 Pre-selected aptamers for enhancing dual-aptamer applications.
An "array-based discovery platform for multivalent aptamers" (AD-MAP) featuring microarray technology was used to enhance the SELEX process for dual-aptamer selection against proteins like angiopoietin-2 (Ang2);[78] sequences from the enriched aptamer pool were first acquired through microfluidic selection and high-throughput sequencing. These sequences were next utilized to construct a custom array and perform parallel affinity assays to identify the strongest Ang2 aptamer ($K_d = 20.5 \pm 7.3$ nM). This aptamer was then complexed with Ang2 to block its primary binding site, and the identical array was employed to identify secondary epitope-binding aptamers. The latter process is challenging, as conventional selection methods typically screen aptamers competing for the same binding site. AD-MAP effectively solved this issue, and Ang2 affinity for the other three isolated secondary aptamers were between 38 and 57 nM.[78] These aptamer pairs were found to be linked to create bidentate probes with >200-fold higher affinity and dissociation constants as low as 97 pM.[78] Microfluidic selection was used to integrate high-throughput affinity-based isolation and partitioning, producing enriched aptamer pools for downstream processing that promoted the dual aptamer applications.

### 2.2.3 ssDNA collection *via* microfluidics.
ssDNA recovery is critical for successive SELEX rounds, and a microfluidic dialysis device that collected ssDNA from double-stranded DNA (dsDNA) at high purity using 25 mM NaOH[79] was shown to be rapid, highly sensitive, and cost-effective. At 0.2 mL h$^{-1}$, the recovery rate was 24%, and the microfluidic approach outperformed manual procedures at higher NaOH concentrations (likely due to faster processing). Alternatively, Lee *et al.*[80,81] produced ssDNAs using droplet-based microfluidics and synthetic, co-polymerizable oligo-microspheres, microspheres of 272 ± 7.1 μm (<3% variation[80]) and 150 ± 13 μm (30 per second with 8.5% variation[81]) were generated, and these particles were covalently attached to acrydite-modified DNA probes for efficient ssDNA amplification *via* asymmetric PCR. Tightly controlled flow rates and optimized channel geometries were critical for generating precisely sized microspheres; this high-ssDNA yield protocol is therefore suitable for automated SELEX and other applications (see Table 1). The collection of ssDNA using microfluidics is a common method to simplify and enhance intermediate SELEX rounds.

## 2.3 Binding and partitioning

Microfluidic platforms have been developed to improve efficiency in both the binding and partitioning steps,[67] and so we discuss these steps together. The key challenge in aptamer selection is rapidly and efficiently isolating high-affinity candidates from a vast pool of sequences that are either in solution or immobilized.

### 2.3.1 Novel SELEX methods using fluidic forces.
Microfluidics offers straightforward hydrodynamic forces for efficient mixing and separation, enabling improved execution of the binding and partitioning steps. For instance, Chang *et al.*[82] introduced Pro-SELEX, a method that could efficiently generate aptamers with desired binding affinities in a single selection round. This approach utilized particle display, emulsion PCR, and a microfluidic device with differential capture zones to sort aptamers based on their target-binding levels. The device demonstrated high capture specificity and could isolate aptamers with different binding affinities. The sorted aptamers were further sequenced and analyzed using the AptaZ algorithm, which compares sequences and selects candidates with the desired binding characteristics. For the human myeloperoxidase (MPO) protein, the first eight aptamers exhibited Z-scores that correlated linearly with binding affinities ranging from 227 pM to 28 nM,[82] and experimental dissociation constant ($K_d$) values differed from the desired one by <25%. The strongest binding affinity was demonstrated by aptamer MPO-16 ($K_d = 166$ pM). Alternatively, I-SELEX instead employs centrifugal acceleration and Dean vortices in spiral microchannels to efficiently separate cell-bound aptamers from unbound nucleic acids.[83] This high-resolution particle separation

**Table 1**  Microfluidic applied in SELEX steps

| SELEX steps | Targets | Major microfluidic techniques | Aptamer characteristics | Duration | Ref. |
|---|---|---|---|---|---|
| Library preparation | XNA polymerase | DrOPs; droplet based microfluidics | n/a | n/a | 74–77 |
| | Ang2 | AD-MAP; microarray | $K_d$: 20.5 ± 7.33 nM (ABA1); $K_d$: 27.6 ± 5.92 nM (ABA65); $K_d$: 97 pM (bidentate ABA1-ABA65) | n/a | 78 |
| | ssDNA | Microdialysis | n/a | n/a | 79 |
| | ssDNA | Droplet based microfluidics | n/a | n/a | 80, 81 |
| Binding/partition | Myeloperoxidase (MPO) | Pro-SELEX; microfluidic sorting, magnetic bead-based, microstructures | Primary selection: $K_d$: ranging 227 pM to 27.8 nM Quantitative selection with desired affinities: $K_d$: 166 pM (MPO-16, the best) Success rate in "great fit (<25% differ from desired $K_d$)" was between 20% and 50% | 1 round (including 3 pre-concentrations) | 82 |
| | var2CSA (variant of the plasmodium falciparum erythrocyte membrane protein 1 (PfEMP1) family); malaria parasite | I-SELEX; inertial focusing; spiral microfluidic channels | $K_d$: ~14 nM (8.1–1); $K_d$: ~84 nM (8.2–1) | 3–4 rounds | 83 |
| | IgE | Microbeads, microstructure, hydrodynamic transfer, integration of affinity selection and amplification | $K_d$: 83.9 nM (enriched pool of candidates) | 2 rounds, 2 h per round | 84 |
| | IgE | Electrokinetic, hydrodynamic, pressure-driven | $K_d$: 12 nM | 4 rounds/10 h | 37 |
| | IgA1 | Electrokinetic, microbeads | n/a | 4 h | 85 |
| | Patient's monoclonal immunoglobulins (M-Ig) | Integrated, IMS; automated, strategic combination | $K_d$ < 50 nM; $K_d$: 36 nM (P3S10) | 12 h | 86 |
| | IgE; bisboronic acid (BA) in glucose | Electrophoretic, microbeads | Against IgE: $K_d$: 10 ± 2.1 nM (SIGE5); $K_d$: 18 ± 3.6 nM (SIGE7); Against BA-glucose: $K_d$: 2 ± 0.7 µM (SBG2); $K_d$: 1 ± 0.5 µM (SBG5) | (3 rounds + counter)/ 10 h | 87 |
| | His-tag & IgE (his-tagged IgE) | Microfluidic SELEX, magnetic bead-based | $K_d$: 26.1 ± 4.9 nM (HisA1-T63); $K_d$: 14.3 ± 3.5 nM (IgEA-T35); LOD: 7.1 nM (dual-aptamer assay of his-tagged IgE in cell culture media in 10 min) | n/a | 88 |
| | IgE | Comparison among conventional, microfluidic chip, and full-chip SELEX | $K_d$: 96.2 ± 9.4 nM (IGE1), $K_d$: 14.5 ± 1.4 nM (IGE1-T) | Conventional/on-chip/ full-chip: 4/1.5/1 days | 89 |
| | Plasmodium vivax lactate dehydrogenase (PvLDH) | Electrodynamic microfluidic channel | $K_d$: range from 31.4 to 97.3 nM; $K_d$: 31.4 ± 3.3 nM (L1); linear dynamic range: 25 fM–2 pM ($R$ = 0.985) and 10–125 pM ($R$ = 0.994); LOD: 7.8 ± 0.4 fM; | 3 h | 90 |
| | G4DNA | GO, electrophoresis, G4DNA binding drug screening | n/a | n/a | 91 |
| | Prostate-specific antigen (PSA) | Acoustofluidics; magnetic beads | $K_d$: 0.7 nM (AS2) | 8 rounds | 92 |
| | IgE | Surface acoustic wave-assisted (SAW); microfluidic chip | $K_d$: 90.8±17.2 nM (full-length); $K_d$: 22. nM (truncated) | 3 rounds in 5 h | 93 |
| | *Candida albicans* (*C. albicans*) | MACD (magnetic force magnetically activated continuous deflection); magnetic nanospheres; microfluidic chip | $K_d$: 21.5 nM (C.al2); $K_d$: 7.9 nM (C.al3) – the best; $K_d$: 50.2 nM (C.al9); $K_d$: 9.2 nM (C.al10) | 6 rounds | 94 |
| | Adenosine | Graphene oxide (GO)-coated magnetic nanoparticles; microfluidic chip | $K_d$: 18.6 ± 1.5 µM | ~2 h per round; 8 rounds | 95 |
| | Transcription factors | SELMAP (SELEX affinity | n/a | 3 rounds | 96 |

**Table 1** (continued)

| SELEX steps | Targets | Major microfluidic techniques | Aptamer characteristics | Duration | Ref. |
|---|---|---|---|---|---|
| | (TFs); Pho4 & AtERF2 | landscape MAPping; microarray-like | | | |
| | Lactoferrin | PMM-SELEX (protein microarray microfluidic SELEX); microarray based; | $K_d$: 1.04 ± 0.50 nM (Lac-6a); $K_d$: 0.63 ± 0.06 nM (Lac-3a); Lac-6a for detection: linear detection range: 0.78–50 µg mL$^{-1}$; LOD: 0.39 µg mL$^{-1}$ | 7 rounds | 97 |
| | Glycated hemoglobin (HbA1c); β-chain hemoglobin (Hb) | Integrated microfluidic chip; magnetic bead | $K_d$: 7.6 ± 3.0 nM (HbA1c aptamer); $K_d$: 7.3 ± 2.2 nM (Hb aptamer) | 5–7 rounds | 98 |
| | Ovarian cancer tissues | Integrated microfluidic system (IMS); microfluidic chip for optimizing ion condition of selection buffer | $K_d$: 266 ± 48 nM (H-45); $K_d$: 920 ± 436 nM (L-25) | 6 rounds | 40 |
| | *Pseudomonas aeruginosa* | Cell-SELEX; microfluidic flow cell | Four primary aptamers selected: JN17, JN21, JN08, JN27; truncated tested: JN17. SH, JN21.SH, JN08.SH; chimeric tested: St21Lp17, St17Lp21, St08Lp17; all $K_d$ ranged from 10–55 nM | 7 rounds | 99 |
| | Porcine aortic endothelial cells expressing KDR (PAE+) | Cell SELEX; dielectrophoresis (DEP) and electrophoresis | n/a | 3 rounds | 100 |
| | Ovarian cancer cell lines: TOV-21G; TOV-122D; BG-1; IGROV-1 | Cell-SELEX; IMS | 2 to 4 aptamers for each cell line selected, $K_d$ ranging from 1.8 nM to 201.3 nM; best affinity aptamer for each cell line: $K_d$: 1.8 nM (21G-2); $K_d$: 22.4 nM (112D-12); $K_d$: 1.3 nM (BG1-10); $K_d$: 10.5 nM (IGR5) | 5 rounds | 101 |
| | Colorectal cancer (CRC); colorectal cancer stem cell (CR-CSC) | Cell-SELEX; magnetic beads; IMS | $K_d$ of eight aptamers ranging from 12.3 nM to 157.2 nM selected; particularly studied: for CRC: $K_d$: 28.5 ± 8.5 nM (HCT-17); $K_d$: 12.3 ± 4.5 nM (HCT-34); for CR-CSC: $K_d$: 27.4 ± 4.9 nM (CSC-16); | 5 rounds | 102 |
| | Ovarian cancer tissues | Tissue-SELEX; on-chip SELEX; automated microfluidic SELEX | $K_d$: 1348.0 nM (cTX-24); $K_d$: 129.2 nM (cTX-36); $K_d$: 178.0 nM (cTX-45) | 6 rounds (1st and 6th are negative selection) | 39 |
| | Ovarian cancer tissues | Tissue-SELEX; phage display; microfluidic chip SELEX | ssDNA aptamer: $K_d$: 53.8 ± 14.9 nM (Tx-01); $K_d$: 2.9 ± 0.8 nM (Tx-02); peptides: $K_d$: 4.8 ± 1.0 nM (Tp-01); $K_d$: 3.2 ± 1.5 nM (Tp-02) | 3 rounds | 54 |
| | Cholangiocarcinoma (CCA) cells; SNU-478, HuCCT-1 | Cell-SELEX; microfluidic chip SELEX, IMS; strategic combination | $K_d$: 29.0 ± 6.8 nM (SN8); $K_d$: 41.0 ± 5.1 nM (HN2); $K_d$: 37.0 ± 5.8 nM (HN16) | 6 rounds | 103 |
| Elution/amplification or others | Not specified | Dual-MAS (dual-microfluidic amplified system); on-chip real-time PCR; microfluidic PCR device | n/a | 30 minutes per round | 104 |
| | XBP1 pre-mRNA | SPR-SELEX; surface plasmon resonance (SPR) | $K_d$: 8 ± 1 nM (sRNA5); $K_d$: 22 ± 4 nM (sRNA1) | 6 rounds | 105 |

approach generated high-affinity aptamers 8.1–1 ($K_d$ = 14 nM) and 8.2–1 ($K_d$ = 84 nM) that could recognize var2CSA protein on malarial parasites and may have potential for use in malarial diagnostics, therapeutics, and vaccine development. These two cases demonstrate that innovative microchannel and/or microstructure designs, combined with hydrodynamic forces, can screen high-affinity aptamers.

**2.3.2 Microbeads and microstructures in microfluidic aptamer selection.** Lin et al.[37,84,85,87] successfully integrated selection and amplification into a single microfluidic SELEX device. Key innovations included using microbeads as the immobile phase, designing weir-like structures to confine microbeads in microchambers, and incorporating thermal control and nucleic acid transport methods to improve
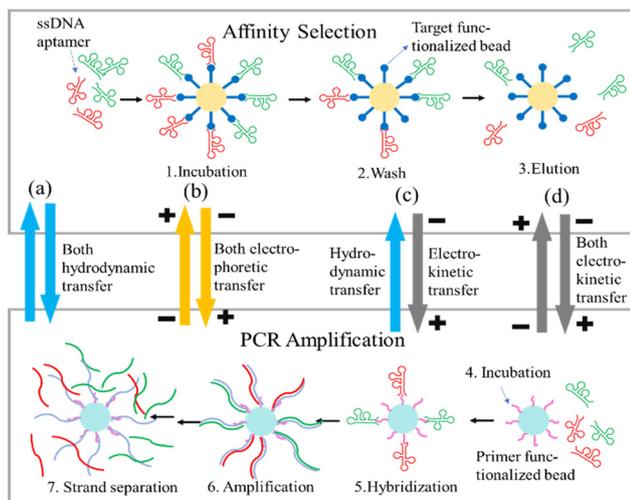
**Fig. 2** An overview of different approaches for transfer on microfluidic chips to enable SELEX cycles. The scheme shows that for on chip SELEX using two separated chambers for affinity selection and PCR amplification. In Lin's group,[37,84,85,87] several works utilized different ways for the aptamers transfer between two chambers within the microfluidic chip. (a) Hilton *et al.*[84] used both hydrodynamic driven transfers (light blue arrowheads). (b) Kim *et al.*[87] displayed both electrophoretic transfer through gel filled channels (yellow arrowheads). (c) Olsen *et al.*[37] in this work used hydrodynamic (light blue arrowhead) plus electrokinetic (gray arrowhead) ways on transfer. (d) In another work, Olsen *et al.*[85] adopted both electrokinetic transfers (gray arrowheads) instead. These critical considerations can increase successful rate on enabling on-chip automated SELEX. The figure concept was adapted from Fig. 1 in ref. 37.

isolation efficiency. These improvements significantly reduced the time, cost, and labor associated with conventional SELEX. Similarly, Hilton *et al.*[84] created a microfluidic chip with two microchambers, one for affinity selection and another for PCR, connected by a serpentine microchannel (Fig. 2a). The chip featured thin-film resistive heaters and temperature sensors for precise thermal control, with target molecules immobilized on microbeads packed in the selection chamber. This approach successfully isolated aptamer candidates with desired temperature-dependent binding characteristics, enhancing the $K_d$ for human IgE to 84 nM after two selection rounds in just 4 h (significantly improving on conventional SELEX).

Alternatively, Kim *et al.*[87] presented a microfluidic approach that integrated the isolation of DNA aptamers through electrophoretic oligonucleotide manipulation (Fig. 2b) within a single chip, allowing the single selection to be completed within ~10 h. The aptamer candidates demonstrated robust binding affinities, with equilibrium dissociation constants of 18 nM or better, showing the technique's versatility in selecting aptamers for both surface-bound and solution-borne targets. Moreover, Olsen *et al.*[37,85] introduced two new microfluidic SELEX technologies to improve aptamer selection efficiency and specificity. The first used electrokinetic and hydrodynamic manipulation in a microfluidic device to immobilize targets and precisely control the selection environment to isolate an IgE

aptamer with a $K_d$ of 12 nM after four rounds of selection in 10 h[37] (Fig. 2c). In the second study, free-solution electrokinetics simplified the SELEX process by actualizing aptamer selection in a continuous flow system[85] (Fig. 2d). The enriched pool of aptamers bound IgA more strongly than the initial random library. This method simplified and accelerated selection, reducing non-specific interactions.

Furthermore, Olsen *et al.*[86] presented a microfluidic device for the rapid isolation of aptamers targeting patient- and tumor-specific monoclonal immunoglobulins in multiple myeloma patients. This device integrated SELEX, counter-selection, and PCR within a closed fluidic loop, reducing the time required per round. After six rounds, an aptamer was identified with a binding affinity of 36 nM, demonstrating the promise of this approach for personalized diagnostics. Similarly, Meng *et al.*[89] compared three SELEX strategies for IgE aptamer isolation. Microfluidic SELEX achieved higher enrichment (4236 counts per million) than conventional SELEX (25 counts per million) after four rounds. The full-chip SELEX method completed isolation in ~12 h; the selected aptamer, IGE1, exhibited high affinity for IgE ($K_d$ = 96 ± 9.4 nM).[89] Microfluidic SELEX reduced reagent consumption, leading to lower costs while enhancing selection stringency and binding. While full-chip SELEX offers integration and automation benefits, chip-selection SELEX is simpler and often provides better PCR efficiency. Finally, another microfluidic SELEX device enabled a 10 min dual-aptamer sandwich assay that detected tag-fused recombinant proteins[88] His-tag and IgE by aptamers screened in 3 and 4 rounds, respectively[88] within 2 days; the limit of detection (LOD) of the former was 7 nM,[88] and the aptamer-functionalized surfaces could be thermally regenerated for up to 20 uses, greatly reducing costs. Collectively, these findings indicate that microfluidic SELEX is a more efficient, cost-effective, and time-saving alternative to traditional SELEX.

**2.3.3 Enhancing screening efficiency by introducing additional force(s).** To further enhance SELEX, researchers have explored integrating additional physical forces within microfluidic platforms. For instance, Chung *et al.*[90] presented a novel method using an electrodynamic microfluidic channel device for rapid aptamer generation. The channel walls were modified with poly-benzoic acid to facilitate the covalent attachment of the malaria protein lactate dehydrogenase (PvLDH). A random pool of ssDNAs was incubated in the device under an alternating current electric field for 60 min, followed by a washing step to remove unbound DNA. The process achieved a high partitioning efficiency of $1.7 \times 10^7$ measured by qPCR, and the resulting aptamers exhibited dissociation constants ranging from 31 to 97 nM. The aptamer-modified sensor effectively detected PvLDH concentrations from 0 to 2 pM at a LOD of only 7.8 ± 0.4 fM.

Alternatively, a microfluidic device was developed to rapidly screen and isolate natural compounds that specifically bind G-quadruplex (G4DNA) using a SELEX-like procedure.[91] This approach integrated an aptamer-carboxyfluorescein/graphene oxide energy transfer optical sensor with on-chip electrophoretic separation, allowing for efficient and rapid screening of active

ligands such as daidzein, berberine hydrochloride, jatrorrhizine hydrochloride, fangchinoline, and a new potential G4DNA active drug, jujuboside A, while demonstrating high sensitivity and effective electrophoretic separation. Microfluidic platforms have also utilized acoustophoresis, which employs acoustic waves to control particles, enabling simultaneous washing and separation of target-bound ssDNA aptamers in continuous flow.[92] This enhances efficiency and specificity, as a sheath flow aligns particles along the channel walls while acoustic forces direct target-bound particles to the center for collection. The continuous flow design improved throughput, and seven aptamers binding prostate-specific antigen were identified; the superior $K_d$ was found to be only 0.7 nM. Integrating acoustophoresis with next-generation sequencing further could also accelerate aptamer selection.[92] Additionally, a surface acoustic wave-enhanced microfluidic chip for aptamer screening demonstrated improved mass transfer, resulting in more effective binding and selection of high-affinity aptamers, including a DNA aptamer that specifically binds IgE within three rounds over 5 h, with a $K_d$ of only ~23 nM.[93]

**2.3.4 Introducing magnetic forces into microfluidic SELEX platforms.** The use of magnetic forces in microfluidic SELEX platforms provides advantages for enhancing aptamer screening efficiency. Magnetic separation *via* superparamagnetic beads enables more efficient washing and partitioning of bound aptamers from unbound ones, improving enrichment. For instance, a magnetically activated continuous deflection microfluidic chip facilitated dynamic selection in continuous flow, allowing simultaneous binding and separation of aptamers.[94] This magnetically activated continuous deflection system pumps targets, a DNA library, and a wash buffer through the chip, with a magnetic field guiding the target-bound sequences. During washing, low-affinity aptamers are removed, and the chip also allowed for the tuning of selection stringency by adjusting target concentrations. Within six rounds of selection, this approach successfully identified a high-affinity aptamer for *Candida albicans* with a 7.9 nM dissociation constant.[94]

Another study reported a microfluidic SELEX method using graphene oxide-coated magnetic nanoparticles (GOMNPs) to select adenosine-specific aptamers.[95] The ssDNA library was incubated with GOMNPs, and adenosine was introduced, allowing specific aptamers to bind. Applying a magnetic field separated the GOMNPs with bound aptamers from unbound ssDNAs. Bound aptamers were then eluted and amplified, and the process was repeated to enrich for high-affinity ones. The microfluidic device enabled efficient, rapid (2 h cycle$^{-1}$) selection, identifying adenosine-specific aptamers with a $K_d$ of ~20 μM (comparable to existing aptamers). Similarly, another study presented a microfluidic system for on-chip SELEX to select aptamers specific to glycated hemoglobin and total hemoglobin.[98] The system automated multiple SELEX steps, reducing time and reagent use compared to traditional methods. The process began with a DNA library incubated with target protein-coated magnetic beads (MBs). High-affinity aptamers were bound to the MBs, which were then separated

*via* a magnet, and the bound aptamers were amplified by PCR. The study successfully selected glycated hemoglobin (HbA1c)- and β-chain hemoglobin (Hb)-specific aptamers with binding affinities of 7.6 ± 3.0 and 7.3 ± 2.2 nM, respectively.

**2.3.5 Advanced SELEX.** "SELEX affinity landscape mapping" (SELMAP) enables high-throughput measurement of transcription factor-binding affinities to diverse DNA sequences.[96] Briefly, a dsDNA library was loaded into the chip, and unbound DNAs were degraded with DNase; bound DNAs were released *via* proteinase K. The recovered oligonucleotides were then PCR-amplified. The approach allowed simultaneous analysis of up to 16 proteins, minimizing reagent use while enhancing throughput. SELMAP's rapid nature, versatility, and precise fluid control make it a powerful tool for understanding gene regulation.[96] Additionally, a SELEX method integrated a protein microarray with a microfluidic chip, enhancing the efficiency and speed of SELEX while allowing quantitative monitoring of aptamer enrichment.[97] This approach successfully identified five high-affinity aptamers for lactoferrin that were specific enough for biosensing and diagnostics.[97]

**2.3.6 Cell- and tissue-SELEX by microfluidic platforms.** Microfluidic platforms have been used for cell- and tissue-SELEX, which allow the selection of aptamers that recognize native target proteins on cells or tissues.[100,101,107,108] For example, DNA aptamers specific for *Pseudomonas aeruginosa* ($K_d$ = 10–55 nM) were demonstrated to effectively bind live bacterial cells.[99] Another study reported a microfluidic chip that combined dielectrophoresis and electrophoresis[100] to effectively remove nonspecifically bound oligonucleotides and found that increasing the flow rate during successive SELEX rounds enhanced selection pressure, yielding aptamers with higher affinities and specificities to the target HEK293 cells.

Another study has reported a microfluidic system for automated on-chip cell-SELEX, which rapidly selected high-affinity aptamers specific to different ovarian cancer (OvCa) cell lines.[101] The system reduced the selection process from 22 to 5 rounds, identifying three aptamers with dissociation constants of 1.3–8.3 nM (comparable to antibodies). Similarly, a compact microfluidic system was reported for aptamer selection against colorectal cancer and colorectal cancer stem cells.[102] This "micro-total-analysis-system" efficiently identified eight aptamers, including three with high affinities ($K_d$ = 12–29 nM), and the selective cell capture rate difference exceeded ~30%. These findings demonstrate the effectiveness of MB-based microfluidic platforms for isolating cancer-specific aptamers with the potential for early diagnosis and targeted therapy. Moreover, an integrated microfluidic system (IMS) capable of automatically identifying aptamers specific to cholangiocarcinoma cells was developed, requiring only 6 rounds of cell-SELEX compared to the typical 15–20 rounds.[103] This system successfully screened three high-affinity aptamers-HN2 (41 ± 5.1 nM), HN16 (37 ± 5.8 nM), and SN8 (29 ± 6.8 nM) that exhibited significant selectivity towards the target cell line.

An innovative microfluidic platform combined tissue-SELEX and phage display technology to rapidly screen cancer affinity reagents for OvCa.[54] This system used a micromixer to wash out weakly bound ssDNA and phages, resulting in selected aptamers and peptides with $K_d$ between 3 and 60 nM (all comparable to typical antibody affinities). The optimal incubation time was 30 min, reducing screening time from 2–3 days to only 5–6 h. The microfluidic chip, which fitted 2 cm tissue slides, showed potential for identifying personalized cancer biomarkers. The same group[39] developed an IMS for efficiently selecting aptamers targeting OvCa tissues by integrating multiple microdevices. This system combined reagents effectively with a mixing index >90% at 50 kPa gauge pressure and a 1 Hz mixing frequency of the micromixer in 4 s. The system also performed 20 PCR cycles in 60 min. Six rounds of tissue-SELEX successfully identified an aptamer with a $K_d$ of 129.2 ± 24.8 nM, indicating strong affinity for OvCa tissues. Moreover, Lin et al.[40] reported another automated microfluidic SELEX system with optimized aptamer selection conditions for tissue in a unique IMS that automatically mixed $Ca^{2+}$, $Mg^{2+}$, $Na^+$, and $K^+$ solutions to create selection binding buffers. Ion species and concentrations could be fine-tuned, and an optimization-SELEX chip improved buffer composition and solution transport, reducing reagent use and human intervention. H-45 and L-25 aptamers passed six optimization-SELEX rounds, and the former exhibited strong affinity (266 ± 48 nM) and specificity for OvCa tissues.

## 2.4 Elution and amplification

Elution is often combined with other steps, namely amplification. For nucleic acid aptamers, heat is commonly used to elute via denaturing, while protein-based SELEX uses competing ligands or buffer exchange since protein could be fragile. After elution, aptamers are amplified via PCR for subsequent selection rounds. For instance, a study introduced a dual-microfluidic amplified system that integrated real-time PCR detection and large-volume PCR amplification within an IMS,[104] enhancing PCR and SELEX efficiency. The system split the enriched library into two streams, and qPCR provided concentration and diversity data in only 30 min with minimal contamination and sample loss by using one stream, while another was amplified for next round selection. It is worth noting that characterizing the selected aptamers is critical yet normally follows SELEX. For example, Dausse et al.[105] developed a microfluidic platform featuring recovery with surface plasmon resonance (SPR), allowing simultaneous selection and evaluation. The study identified RNA aptamers forming stable loop–loop complexes ($K_d$ = 8 nM), and high-throughput sequencing revealed candidates binding 79 times faster than those with fully complementary loops. A comprehensive table for providing an overview of the advantages and disadvantages of various microfluidic SELEX techniques and quick comparisons is listed in Table 2.

# 3. IMS for SELEX–based aptamer selection

## 3.1 Challenges in aptamer selection and SELEX

The primary objective of SELEX is to discover aptamers that exhibit both high affinity and specificity, and this can be achieved via SELEX[66] and alternative[67] methods (Table 3). The former is lengthy, and the selected ssDNAs must confirm to rigid specificity and affinity requirements. The prolonged operational duration represents the most significant bottleneck, and researchers are exploring methods to increase efficiency. One such approach is microfluidic SELEX, which can automate and accelerate the selection process. By reducing the number of cycles and enhancing the interaction between aptamers and target molecules, microfluidic SELEX offers a promising solution to the time-consuming, labor-intensive nature of traditional methods. Additionally, advancements in bioinformatics are aiding in the design of aptamers with improved affinity and specificity, further streamlining the selection process.

## 3.2 IMS for aptamer selection

**3.2.1 Benefits of integrated microfluidic SELEX systems.** IMS present numerous benefits over conventional SELEX methods. Firstly, IMS facilitate automated, rapid, and continuous (rounds of) SELEX,[40] thereby enhancing the identification of candidate aptamers. Furthermore, should the initially selected aptamer fail to satisfy the criteria during subsequent validation, a new selection process can be swiftly commenced. Prior IMS methods have employed straightforward, pressure-driven, and electrokinetic transport mechanisms to facilitate the interactions between ssDNA libraries and target molecules.[87] Furthermore, a novel, integrated SELEX method has been established that employs target-bead affinity selection and facilitates automated liquid transport to isolate specific aptamers without the need for off-chip procedures. Other IMS feature MBs, immobilization of affinity agents onto substrates, employment of external devices (e.g., pneumatic, electrical, or magnetic forces) to manage mixing and movement of substrates, automation of binding, washing, and enrichment, and the implementation of various SELEX methodologies, which will be reviewed in the following sections.

**3.2.2 MBs in aptamer selection.** Aptamers can be conjugated to a variety of materials, such as MBs,[101] gold,[109] nanogold,[110] polymeric resins,[111] and polystyrene,[112] for application in on-chip diagnostics. MBs with surface-modifiable functional groups also possess the ability to bind nucleic acids, proteins, antibodies, biomolecules, and cells, rendering them suitable for the selection of aptamers.[62] The small, mobile nature of MBs facilitate their movement within fluids, allowing them to traverse different chambers across various processing stages. Furthermore, their significantly greater surface compared to the flat surfaces of chambers enhances the likelihood of successful capture of candidate ssDNA. Therefore,

**Table 2** Overview of microfluidic SELEX techniques

| Microfluidic technique | Advantages | Disadvantages | Typical applications |
|---|---|---|---|
| Pro-SELEX | - Single-round selection<br>- High capture specificity | - Requires complex microfluidic devices<br>- Needs specialized algorithms for analysis | Protein targets (e.g., MPO) |
| I-SELEX | - Efficient separation of cell-bound aptamers<br>- High-resolution particle separation | - Limited to cell or particle-based targets<br>- May require multiple rounds | Cell surface proteins (e.g., var2CSA) |
| Microbead-based SELEX | - Integration of selection and amplification<br>- Reduced time and reagent consumption | - Potential for non-specific binding to beads<br>- May require optimization of bead size/type | Protein targets (e.g., IgE, IgA) |
| Electrophoretic SELEX | - Continuous flow system<br>- Reduced non-specific interactions | - Limited to charged molecules<br>- May require careful buffer optimization | Small molecules and proteins |
| Acoustic wave-enhanced SELEX | - Improved mass transfer<br>- Simultaneous washing and separation | - Requires specialized acoustic equipment<br>- May have limitations with certain sample types | Proteins and cells (e.g., PSA, IgE) |
| Magnetic bead-based SELEX | - Efficient target immobilization and separation<br>- Compatibility with various targets | - Possible magnetic bead aggregation<br>- May require optimization of magnetic field strength | Proteins, cells, and small molecules |

in many integrated microfluidic chips (IMC), MBs are commonly employed as the target carrier for SELEX selection of specific aptamers.

### 3.3 IMC SELEX types

The IMC depicted in Fig. 3 can be categorized to four types: simple SELEX, complex SELEX, conditional SELEX, and *in vivo*-like SELEX. The former entails immobilizing affinity agents onto a planar substrate and employing fluid flow to facilitate the processes of binding, washing, and enrichment for the selection of candidate ssDNAs. This process is commonly referred as "positive selection". Furthermore, IMC may further incorporate MBs to augment the likelihood of interactions between ssDNA and affinity agents, thereby increasing the yield of captured aptamers. Conventional SELEX usually involves >20

rounds of selection, while simple, on-chip SELEX may require only 4–5.[36,113,114]

IMC can employ external devices like pneumatic, electrical, or magnetic forces[62,115,116] to manage the mixing or movement of substrates (or MBs) within the fluid. This can occur in a single or back-and-forth manner to speed up reaction times or facilitate ongoing selection processes (discussed in detail below). The simple SELEX method relies on incubation of probe-coated MBs (or planar substrates) with random ssDNA libraries (Fig. 3A). The target-bound MBs are then collected *via* magnet, and unbound ssDNAs are removed. The collected ssDNAs are enriched *via* PCR. These steps constitute a single positive selection round. After several rounds, high-affinity aptamer candidates are obtained (Fig. 3A). Consequently, microfluidic SELEX chips continuously and automatically perform multiple rounds of SELEX for screening various specific aptamers, targeting molecules such as Hb[98] and C-reactive protein.[36]

**Table 3** Current aptamer selection methods

| | | | |
|---|---|---|---|
| Non-SELEX[67] | 1. *In silico* aptamer design<br>2. High-throughput screening<br>3. Phage display method<br>4. Ribosome display method<br>5. CE based (NECEEM, ECEEM)<br>6. Competitive<br>7. Centrifuge based | | |
| SELEX[66] | 1. Non-chip SELEX | a. Conventional SELEX<br>b. Bead-based SELEX<br>c. Plate-based SELEX<br>d. *In silico* and computational SELEX | |
| | 2. Chip SELEX | a. On-chip SELEX<br>b. Lab-on-a-chip SELEX | |
| | | c. Microfluidic SELEX | i. Droplet-based SELEX<br>ii. Continuous-flow SELEX<br>iii. Paper-based SELEX<br>iv. Digital SELEX |
| | | d. Integrated microfluidic devices for SELEX | i. Simple SELEX<br>ii. Complex SELEX<br>iii. Conditional SELEX<br>iv. *In vivo*-like SELEX |
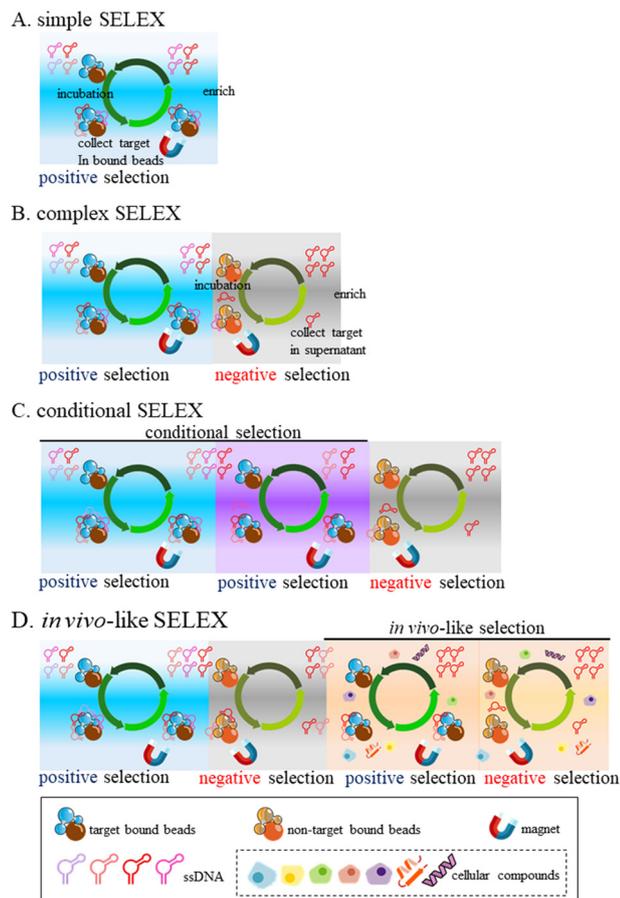
**Fig. 3** Aptamer selection methods in integrated microfluidic chip. (A) The core of IMS is simple SELEX, commonly referred to as positive SELEX which already integrated necessary steps for SELEX cycles. (B) Complex SELEX combines positive and negative SELEX to enhance aptamer performance. (C) Conditional SELEX varies the sequence and number of positive and negative SELEX to improve specificity and affinity. (D) More complex strategies, like *in vivo*-like SELEX, enable aptamer screening in ambient environments, isolating aptamers that may retain functionality in complex conditions, such as therapeutic applications.

**3.3.1 Complex SELEX.** To enhance specificity, "negative selection" may be employed. In this process, structurally analogous molecules capture ssDNAs with diminished specificity, while aptamers exhibiting higher specificity remain in the supernatant after separation.[117] By implementing multiple cycles of positive and negative selection, more specific aptamers with high affinity can be obtained *vs. via* positive selection alone (*i.e.* simple SELEX) (Fig. 3B).[118,119] Incorporating of negative selection could improve aptamer specificity by removing non-specific binders, decreasing off-target interactions, and increasing affinity in complex environments. However, it adds complexity and screen time to the selection process and may exclude valuable aptamers due to over-stringency. As a result, while it improves target specificity, careful optimization is required to avoid restricting the diversity of the aptamer pool.

**3.3.2 Conditional SELEX.** ssDNAs are susceptible to conformational changes induced by ion type and concentration, pH, temperature, and other factors (Table 4).[120–129] To enhance

stability of the screened aptamers, several strategies for chemical and structural modifications can be employed. These include (1) chemical modifications,[130–132] such as 2′-*O*-methyl RNA, locked nucleic acids, or phosphorothioate linkages, which can improve the stability of aptamers by increasing their resistance to nuclease degradation and enhancing binding affinity; (2) PEGylation,[133] which increases molecular weight, reduces renal clearance, and enhances stability in fluids; (3) backbone modifications,[134,135] where the sugar-phosphate backbone of aptamers is altered using peptide nucleic acids or morpholinos (thereby significantly enhancing resistance to enzymatic degradation & improving stability); (4) aptamer dimerization and multi-merization,[136] which involves linking multiple aptamers together and can enhance binding affinity and stability through cooperative effects; and (5) G-quadruplex stabilization,[137] which contributes to the structural integrity and functionality of aptamers (as examined through post-SELEX processing). Future developments in bioinformatics, crystallography, and 3D structure analysis are anticipated to facilitate more accurate assessments of aptamer-target interactions, thereby improving the selection process.

SELEX must be performed under diverse conditions to ensure that aptamers screened *in vitro* are effective/accurate in real life scenarios. IMC allows for automation and concurrent performance evaluation under various conditions, supporting the continuous and condition-specific SELEX of aptamers that are customized to meet the demands of subsequent assays. Conditional SELEX, which involves alternating positive and negative selection as well as the incorporation of various conditions throughout the selection process, can be further refined through the application of broad or condition-specific positive and negative selection strategies. For instance, IMC can automate and control the types and concentrations of ions (*e.g.*, $Mg^{2+}$, $Na^+$, $K^+$, $Ca^{2+}$) and other critical factors within each chamber. This capability is particularly important given the differences between the microenvironments of cancer and normal cells, as a dedicated IMC facilitated the selection of a specific aptamer for ovarian cancer (Fig. 3C).[40] Methodologies that utilize the structural-switching characteristics of aptamers in response to varying environmental conditions, namely different ion concentrations, have been designed to differentiate influenza A from influenza B viruses.[138]

**3.3.3 *In vivo*-like SELEX.** The complex nature of natural environments means that reliance solely on conditional SELEX may be insufficient for the identification of aptamers that meet the diverse conditions necessary for clinical detection or therapeutic applications. For instance, the tumor microenvironment[139] differs markedly from that of normal cells. Due to rapid proliferation, altered metabolism, and metastatic behavior of cancer cells, factors such as pH, ion concentrations, lactate levels, and the presence of associated cells and molecules are significantly modified.

Numerous microfluidic investigations employing tumor-on-a-chip technology have concentrated on the advancement of anti-cancer pharmaceuticals.[140] The use of aptamer-containing microfluidic chips for detecting circulating tumor cells

**Table 4** Factors influencing ssDNA conformation

| Factors | Effects on conformation | Ref. |
|---|---|---|
| Ion species and concentration | Stabilizes or destabilizes secondary structures<br>1. Cations (*e.g.*, $Mg^{2+}$, $Na^+$, $K^+$)<br>These stabilize the negative charges on the phosphate backbone, facilitating folding and the formation of secondary structures like hairpins or loops<br>2. Anions<br>Influence nucleic acid stability and folding through ionic interactions | 62 |
| pH | Alters base protonation, affecting hydrogen- bonding<br>1. Acidic pH<br>To protonate nucleobases, altering hydrogen- bonding patterns and thus affecting secondary structure formation<br>2. Alkaline pH<br>Lead to deprotonation, affecting base-pairing and possibly leading to strand denaturation or misfolding | 98 |
| Temperature | Denatures or stabilizes secondary structures<br>1. High-temperature<br>Causes denaturation of secondary structures, leading to a more linear conformation<br>2. Low-temperature<br>Promotes the formation of secondary structures through stable base-pairing | 36 |
| Molecular crowding | Promotes compact folding through excluded volume effects | 118 |
| Solvent conditions | Affects hydration and hydrogen bonding<br>1. Water activity<br>Lower water activity can stabilize certain nucleic acid structures by reducing the hydration shell<br>2. Organic solvents (*e.g.*, ethanol, DMSO)<br>Disrupt hydrogen bonds and affect the overall stability of the secondary structure | 119 |
| Base sequence and composition | Influences base-pairing and structural stability<br>1. GC content<br>Higher GC content typically increases stability due to stronger hydrogen-bonding<br>2. Sequence repeats and palindromes<br>Lead to the formation of specific secondary structures such as hairpins or cruciform structures | 120 |
| Secondary structure formation | Hairpins, loops, bulges, and G-quadruplexes<br>1. Hairpins, loops, and bulges<br>These structures form based on complementary base-pairing within the strand and are influenced by the factors mentioned above<br>2. G-Quadruplexes<br>These are formed by guanine-rich sequences and are stabilized by the presence of specific cations like potassium | 121 |
| Chemical modifications | Alter base pairing and backbone flexibility<br>1. Methylation or alkylation<br>Alter base-pairing properties and overall conformation<br>2. Phosphorothioate linkages<br>These modifications in the backbone can influence the flexibility and binding interactions of nucleic acids | 122 |
| Binding proteins or ligands | Induce specific conformations | 123 |
| Mechanical forces | Modify structure through stretching or twisting | 124 |

(CTCs),[141,142] exosomes,[143,144] and modeling 3D environments[145,146] have also become an emerging trend in cancer diagnostics.[147,148] Epigenetic biomarkers have also been employed in liquid biopsies to facilitate the early diagnosis and prognosis of cancer.[149] For instance, a microfluidic system was utilized for the screening of aptamers in conditions that simulated diverse tumor microenvironmental conditions in patient blood (Fig. 3D), and highly specific, methylated BRCA1 and BRCA2 aptamers suitable for clinical applications were identified through an *in vivo*-like SELEX approach.[150]

### 3.4 Summary

Aptamer-based microfluidic systems represent a significant advance in clinical diagnostics, offering high specificity, sensitivity, and versatility for identifying a wide range of

biomarkers. These technologies are poised to play a crucial role in the future of clinical diagnostics, providing tools for early detection, personalized treatment, and continuous monitoring of cancer and other diseases. It is envisioned that advancement of microfluidic SELEX may open up great opportunities for screening and applications of aptamers.

Various SELEX methodologies have distinct advantages and limitations. Conventional SELEX offers versatility across various targets but faces challenges with long selection times and PCR-induced biases. Magnetic bead-based SELEX improves binding efficiency and microfluidic integration but requires optimization for specificity. Droplet-based SELEX enables high-throughput screening with minimal reagent use, particularly effective for small molecules and proteins, though complex device microfabrication may limit its practical use. Capillary electrophoresis SELEX excels in

precise complex separation but faces issues such as scalability challenges. On-chip SELEX reduces selection rounds and automates processes, while conditional SELEX improves clinical relevance by incorporating physiological conditions. Researchers can select optimal methods based on target complexity, application needs, and available resources.

# 4. Non-SELEX

## 4.1 Alternative methods for aptamer selection

**4.1.1 Introduction.** Alternative techniques have emerged recently that address limitations such as PCR in SELEX, which was referred as "non-SELEX" to distinguish them from amplification-based approaches associated with conventional SELEX. By avoiding PCR, amplification biases caused by varied template sequence composition preferences may be avoided.[17,151] Additionally, there is no need to convert PCR products back to ssDNA, and integration into IMS is simplified on account of the reduced need for precise thermal control, thus shortening the total SELEX time.[17,151] Non-SELEX methods generally utilize high-resolution partitioning techniques like CE and/or implementing microfluidics to directly isolate aptamers based on their binding affinity. Therefore, it can enhance efficiency and reduce time and costs.[45,152,153] Non-SELEX methods can significantly improve selected pool affinity in just hours, compared to days or weeks for SELEX.[154] Additionally, strategies to minimize or eliminate fixed primer regions have been developed to reduce non-specific binding and false positives.[155,156] These advancements, along with high-throughput analyses, are expected to accelerate the development of aptamers for biosensing, diagnostics, and therapeutics[47,67,157] (Fig. 4). Because of the lack of amplification cycles, non-SELEX methods risk missing low-abundance but high-affinity aptamers. Furthermore, the lack of iterative selection limits the ability to differentiate between high- and low-affinity binders, lowering the sensitivity of the screening process. Despite the efficiency of SELEX, its reliance on amplification might introduce biases and could limit throughput of the screening. Alternatively, Non-SELEX methods address these challenges by utilizing direct selection strategies.

**4.1.2 CE-based non-SELEX.** CE-based non-SELEX technologies were developed to select aptamers without amplification.[56,158,159] One such method, "non-equilibrium capillary electrophoresis of equilibrium mixtures,"[152,154] separated oligonucleotide-target complexes from free oligonucleotides and reduced the selection period to an hour. To overcome the limitations of SELEX, including amplification bias and challenges with RNA/XNA libraries, the development of Non-SELEX alternatives has been reported.[49,157,160] Other methods include MB-assisted screening,[161] which also offers more streamlined and cost-effective selection.

## 4.2 Non-SELEX methods: applications and advancements

**4.2.1 Non-SELEX in mobile formats.** Aptamer selection can be conducted in either immobilized or non-immobilized manners for non-SELEX;[67] each has distinct advantages and
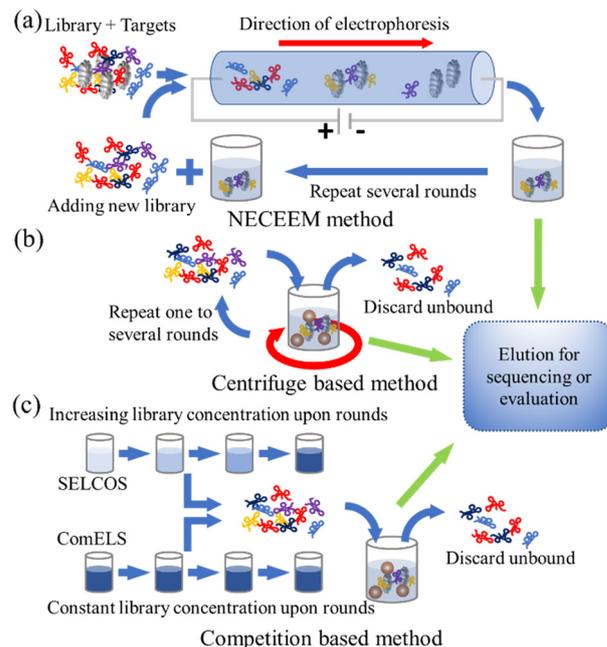


**Fig. 4** Schematic overview of non-SELEX methods. (a) Working principle of non-equilibrium capillary electrophoresis of equilibrium mixtures (NECEEM). (b) Overview of centrifuge-based method, the targets should be able to separate from free diffusing library. (c) Competition based method overview, including systematic evolution of ligands by competition-enhanced ligand selection (SELCOS) and competition-enhanced ligand selection (ComELS).

disadvantages. As an example of the latter, fluorescence anisotropy and CE enabled isolation of high-affinity DNA aptamers targeting tau protein isoforms at a 28 nM detection limit,[162] without the need for PCR. Another selection pressure-controlled CE approach yielded aptamers for holo-transferrin (H-Tf) and platelet-derived growth factor-BB with $K_d$ of 50 and 81 nM, respectively.[163] This method featured one round of pressure-controllable selection that relied on high-efficiency separation, single round selection, and target competition with controllable pressure via balanced or dominant protein competition. Alternatively, centrifugation-based partitioning rapidly selected E. coli-specific aptamers with $K_d$ values as low as 4 nM.[164] This method isolated aptamers by serially removing unbound DNA from a mixture of bacteria and DNA libraries via centrifugation, followed by separation and cloning of target-bound DNA. A similar approach with E. coli involved a dual-aptamer colorimetric assay and was characterized by a 10 CFU mL$^{-1}$ detection limit.[165] Finally, another centrifugation-based approach including positive and negative selection stages isolated aptamers targeting airborne *Citrobacter braakii* with $K_d$ values of 16 and 27 nM, in liquid and air, respectively.[166] (Table 5).

**4.2.2 Non-SELEX methods in immobilized formats.** The most obvious and well adapted format for immobilized Non-SELEX is bead-based partitioning. For instance, a MB-based method rapidly selected β-casomorphin-7 aptamers, including one with a 29-nM $K_d$.[172] Several other studies were instead based on competitive selection. For instance, the "competition-

**Table 5** The research works of non-SELEX methods reviewed in the past five years

| Reference | Main method | Target | Aptamer performance |
|---|---|---|---|
| Tapp et al.[167] | Competition-enhanced ligand selection (CompELS) | PlanarAu, non-biological targets | $K_d$ = 0.56 nM for high affinity aptamer |
| Lisi et al.[162] | Non-SELEX-based aptamer selection, fluorescence anisotropy | Tau proteins (t-441, t-381, t-352, t-383) | $K_d$: 13 ± 3 nM for t-441 aptamer, 116 ± 6 nM for t-381 aptamer, 84 ± 6 nM for t-352 aptamer, 49 ± 4 nM for t-383 aptamer; LOD: 28 nM for t-441, 3.2 nM for t-381, 6.3 nM for t-352, 22 nM for t-383 |
| Sullivan et al.[168] | Secondary structure analysis of DNA aptamers | Gold nanorods | Multiple secondary structure families identified |
| Kushwaha et al.[169] | Systematic evolution of ligands by COmpetitive selection (SELCOS); competitive non-SELEX for rapid aptamer enrichment | Influenza virus subtype-specific aptamers | High selectivity, $K_d$ = 82 pM for H1N1 and 88 pM for H3N2 |
| Kim et al.[164] | Non-SELEX-based aptamer selection | *Escherichia coli*, specific bacterial strains | $K_d$: 3.9 nM for 20–5 aptamer, 8.0 nM for 20–7 aptamer, 10.1 nM for 20–10 aptamer; specific binding to *E. coli*, negligible binding to other bacteria |
| Wu et al.[170] | Flow-cell-based massively parallel aptamer characterization | Base-modified DNA aptamers | $K_d$: 3.3 nM for aptamer VEGF-4, 16.9 nM for aptamer SL2B; screening of aptamers in human serum conditions |
| Yang et al.[163] | One-round pressure-controllable aptamer selection | Human holo-transferrin, PDGF-BB | $K_d$: 81 nM for PDGF-BB, 50 nM for holo-transferrin, improved specificity and affinity using competitive pressure selection |
| Biyani et al.[171] | Competitive selection for DNA aptamer inhibition of CYP24 | CYP24A1 (cancer-related enzyme) | Inhibition: 41% of CYP24 endogenous activity |
| Liu et al.[165] | Non-SELEX-based aptamer selection | *Escherichia coli* | $K_d$: 101.76 nM for aptamer 2–17–2, LOD: 10 CFU mL$^{-1}$, specificity: excellent selectivity over other bacterial strains such as *S. aureus*, *V. parahaemolyticus*, and *L. monocytogenes* |
| Parashar et al.[172] | Non-SELEX-based magnetic bead approach | β-Casomor-phin-7 peptide | $K_d$: 28.93 ± 0.783 nM for aptamer Seq. ID no. 3 |
| Jeong et al.[166] | Non-SELEX-based aptamer selection | *Citrobacter braakii* (airborne bacteria) | CB-5 aptamer: $K_d$: 16.42 nM in liquid culture, 26.91 nM in aerosolized samples; LOD: for liquid culture, 1.8 × 10$^3$ CFU mL$^{-1}$, for aerosol 1.6 × 10$^3$ CFU mL$^{-1}$; high specificity for *C. braakii* |
| Lozoya-Colinas et al.[173] | Parallelized library screening for XNA aptamers | SARS-CoV-2 S1 protein (spike protein) | $K_d$: sub-nanomolar affinity, 0.8 to 3.7 nM; enhanced specificity against off-target proteins (HSA and SA); excellent target discrimination |
| Yoshikawa et al.[174] | Massively parallel screening platform for molecular switches | Aptamers converted to molecular switches | For ATP, $K_d$: ranged from 12–157 μM; for glucose, $K_d$ is 1.9 mM for aptamer NNG, over 8000 aptamer switches exhibiting >2-fold fluorescence intensity change |

enhanced ligand selection" (ComELS) approach identified high-affinity DNA aptamers ($K_d$ = 560 pM) for non-biological targets, demonstrating the potential for microfluidic integration to reduce selection cycles.[167] Further analysis of these aptamers' secondary structures provided insight into how they would be bound to gold nanorods.[168] Another competitive method, "systematic evolution of ligands by competitive selection (SELCOS)," rapidly enriched DNA aptamers specific to influenza virus subtypes, exhibiting $K_d$ of 82 and 88 pM for H$_1$N$_1$ and H$_3$N$_2$, respectively; this approach could complement microfluidic-based sensor development.[169] Similarly, SELCOS also identified a novel DNA aptamer that selectively inhibited CYP24A1, achieving sub-nM $K_d$ values and showing potent anti-proliferative activity in cancer cells.[171] These studies demonstrate the versatility and efficiency of non-SELEX methods across diverse targets and platforms (Table 5).

There are a few difficult-to-categorize but worthwhile methods worth mentioning. For instance, flow cell-based

screening on a modified Illumina MiSeq platform allowed parallel analysis of base-modified DNA aptamers, achieving $K_d$ values of 3.3 and 16.9 nM for VEGF and SL2B aptamers, respectively.[170] A single-round screening method produced XNA aptamers targeting the SARS-CoV-2 S1 protein with affinities between 0.8 and 3.7 nM.[173] These two cases used modified DNAs, which are difficult to incorporate into other SELEX methods. Additionally, a parallel platform for converting aptamers into molecular switches was associated with $K_d$ values from 12 to 157 μM, offering the potential for biosensor development.[174] These advances demonstrate the growing capabilities in aptamer screening and characterization for therapeutic and diagnostic applications (Table 5). Non-SELEX methods rely on the high efficiency of partitioning *via* hydrodynamic, magnetic, or electrokinetic forces and are particularly suitable for integration with microfluidics. Utilizing platforms with innovative materials or specialized microstructures can improve their performance. The

miniaturization and automation of non-SELEX processes on a chip may enable high-throughput, rapid, and more resource-efficient aptamer discovery.

# 5. Versatility of aptamer-based detection strategies *via* microfluidics

## 5.1 Detection of a wide range of targets by aptamers

Aptamers offer advantages over traditional antibodies, including chemical stability and ease of 1) synthesis, 2) modification, and 3) tissue penetration.[175,176] Aptamers have been successfully applied to detect ions, small molecules, proteins, viruses, and cells.[177,178] This structural based versatility[179–181] has led to the development of aptamer-based biosensors for pathogen detection,[182] disease diagnosis,[183,184] food safety,[185] and environmental monitoring.[186,187]

## 5.2 Ions and chemical compounds

**5.2.1 Ions.** Aptamer and microfluidics have been used for detection of various ions. For instance, an IMC combined with MB-tagged aptamer probes for performing multibranched hybridization chain reactions was developed for high-throughput, multiplex detection of kanamycin, 17β-estradiol, and lead ions in food samples.[188] Another study developed an IMC that integrated solid-phase extraction with a graphene-oxide quantum dot array for automated, high-sensitivity detection of $As^{3+}$, $Cd^{2+}$, and $Pb^{2+}$, achieving low detection limits ($K_d$ = 5–41 nM) across a wide dynamic range within 45 min.[189] Similarly, a microfluidic sensor featuring graphene-oxide and FAM/HEX-labeled DNA aptamers achieved highly sensitive detection of $Hg^{2+}$ and $Pb^{2+}$ in water, with LODs of 0.7 and 0.5 ppb, respectively.[190] Another study utilized an electrochemical paper-based microfluidic chip for detecting ions, achieving LODs of 23 pM for $Cd^{2+}$ and 46 pM for $Pb^{2+}$, with a detection range of 0.1–1000 nM.[191] In another work, the researchers employed a DNA aptamer-linked hydrogel integrated with a microfluidic heating system for repeatable detection of silver ($Ag^+$) ions, offering a detection range from 10 μM to 10 mM, with repeatability across three cycles.[192] Similarly, another group developed a dual-modality aptasensor for detection of mercury,[193] and the microfluidic device demonstrated an LOD of 0.01 ppm (linear range = 0.01 to 1 ppm) for electrochemical detection, and a colorimetric limit of 0.5 ppm (0.5 to 20 ppm). Finally, a microfluidic aptasensor point-of-care (POC) device was developed for determining $K^+$ concentration in chronic kidney disease patient blood (LOD = 0.01 mM).[194] More detail information could be found in Table 6.

**5.2.2 Chemical compounds.** Chemical compounds can also be detected using aptamer-based microfluidic sensors. For instance, a study has demonstrated the use of olfactory receptors immobilized by anti-His6-tag aptamers to detect diacetyl with high specificity and a 0.01 nM detection limit.[195] Microfluidic electrochemical aptasensors have also been developed for detecting polychlorinated biphenyls like

3,3′,4,4′-tetrachlorobiphenyl (PCB77) using exonuclease I and DNA/AuNPs/HRP nanoprobes (LOD = 9 pg $L^{-1}$).[196] Another microfluidic ratiometric electrochemical aptasensor was developed for detecting PCB77 with a broad detection range (0.1 pg $mL^{-1}$–1000 ng $mL^{-1}$) and an exceptionally low LOD of 0.16 fg $mL^{-1}$.[197] Moreover, smartphone-integrated aptasensors employing gold-coated polystyrene microparticles have demonstrated rapid, label-free, and selective detection of pesticides like imidacloprid and carbendazim, achieving LOD as low as 3 and 1.5 ppm, respectively, within a 0.39 to 100 ppm range[198] (Table 6).

## 5.3 Small molecules and biomolecules

**5.3.1 Antibiotics.** Various studies have demonstrated the versatility of microfluidic-based aptasensor technologies for detecting a wide range of antibiotics and contaminants. For instance, Chen *et al.*[199] utilized a graphene-based field-effect transistor sensor to achieve ultra-sensitive detection of tobramycin, with an LOD of 0.3 nM and a detection range of $10^{-8}$ to $10^{-4}$ M. Another group developed a IMC-based ratiometric aptasensor using rolling circle amplification for kanamycin detection, reaching an LOD of 0.3 pg $mL^{-1}$ (range = 0.8 pg $mL^{-1}$ to 10 ng $mL^{-1}$).[201] The same team also introduced a simultaneous detection method for kanamycin, aflatoxin M1, and 17β-estradiol using a magnetic tripartite DNA aptasensor, with LODs of 0.3, 1, and 7 pg $mL^{-1}$, respectively.[204] Alternatively, another group demonstrated a localized SPR sensing chip for detecting enrofloxacin at an LOD of 0.001 ng $mL^{-1}$ and a range of 0.01–100 ng $mL^{-1}$.[210] For the same target, Tian *et al.* presented a lateral flow aptasensor using gold nanoparticles (AuNPs) for enrofloxacin detection, with mobile phone-based readout for on-site analysis.[206] The sensor showed an LOD of 0.1 μg $L^{-1}$ and a detection range of 0.1–$10^4$ μg $L^{-1}$. These studies highlight advancements in microfluidic aptasensors and their high sensitivity across broad detection ranges and differing applications (Table 6).

**5.3.2 Toxins.** Several groups have developed microfluidic technologies for detecting toxins, including ochratoxin A (OTA) and aflatoxin M1. For instance, Costantini *et al.*[200] used a lab-on-chip system with an aptasensor to achieve an OTA detection range of 5–200 ng $mL^{-1}$ and an LOD of 1.3 ng $mL^{-1}$ Similarly, Nekrasov *et al.*[202] developed a graphene field-effect transistor for on-chip OTA detection, reaching an LOD of 4 pg $mL^{-1}$ at a range of 10 pg $mL^{-1}$ to 4 ng $mL^{-1}$. Khoshbin *et al.*[207] also developed a liquid crystal-based aptasensor using a π-shaped DNA structure for ultra-low detection of OTA. The sensor achieved a detection limit of 0.63 aM, with high selectivity testing in grape juice, coffee, and human serum. Moreover, another group designed a ratiometric thermal-regulated sensor with a COF-Au-MB-Apt signal probe for detecting OTA as well.[211] The sensor achieved an LOD of 0.12 pg $mL^{-1}$ and a detection range of 0.2 pg $mL^{-1}$ to 0.6 μg $mL^{-1}$, with 98.5% regeneration efficiency over seven cycles. For aflatoxin M1, Kasoju *et al.*[205] micro-fabricated a microfluidic paper-based

**Table 6** List of research works using aptamers targeting ions to small molecules

| Targets | Microfluidic methodology | Detection performance | Ref. |
|---|---|---|---|
| Mixed, small molecule, lead ion, kanamycin, 17β-estradiol | Microfluidic chip (MC); magnetic bead (MB); multibranched hybridization chain reaction (mHCR) | Detection limits: $1.76 \times 10^{-4}$ nM (kanamycin), $1.18 \times 10^{-4}$ nM (17β-estradiol), $1.29 \times 10^{-4}$ nM, ($Pb^{2+}$); linear range: $5.89 \times 10^{-4}$–10 nM (kanamycin), $3.94 \times 10^{-4}$–3.5 nM (17β-estradiol), $4.29 \times 10^{-4}$–3.5 nM (lead ion); sensor reusable for 4000 samples; temperature and pH sensitive, reaction time for mHCR needed | 188 |
| $As^{3+}$, $Cd^{2+}$, $Pb^{2+}$ | Solid-phase extraction (SPE); micropump, micromixer; graphene oxide quantum dot (GOQD) array chip; DNA aptamer | Detection limits for $As^{3+}$ (5.03 nM), $Cd^{2+}$ (41.1 nM), $Pb^{2+}$ (4.44 nM); linear range: $As^{3+}$ (0.1 μM to 10 mM), $Cd^{2+}$ (1 μM to 10 mM), $Pb^{2+}$ (1 μM to 10 mM); recovery efficiency >80%; pH-dependent metal adsorption | 189 |
| Hg(ɪɪ)($Hg^{2+}$), Pb(ɪɪ)($Pb^{2+}$) | T-type micromixer with a tortuous channel; PDMS microfluidic device; graphene oxide (GO); DNA aptamer with FAM or HEX fluorescent dyes | Hg(ɪɪ): linear range: 10–250 nM or 2.0–50 ppb, LOD: 0.70 ppb; Pb(ɪɪ): linear range: 10–100 nM or 2.1–20.7 ppb, LOD: 0.53 ppb | 190 |
| $Cd^{+2}$, $Pb^{+2}$, | Electrochemical paper-based microfluidic chip; Gold nanoparticles (AuNP); DNA aptamer paper-based microfluidic analytical devices (μPADs) | LOD: 46.23 pmol $L^{-1}$ for cadmium ($Cd^{2+}$); LOD: 23.31 pmol $L^{-1}$ for lead ($Pb^{2+}$); detection linear range from 0.1 nmol $L^{-1}$ to 1000 nmol $L^{-1}$; detection in just 15 minutes; stay good at −20 °C for 5 days; chip recovery rate of 93.20% to 95.80%; not used in extreme pH | 191 |
| $Ag^+$ | DNA aptamer-linked hydrogel; sensor: hydrogel, micro-heater, and micro-channel; aptamers cross-linked to acrylamide hydrogel | Concentration range ($10^{-5}$–10 mM); Concentration dependent shrinking ratio ($\varepsilon$) of DNA aptamer-linked hydrogel; stable at temperatures (4–100 °C) | 192 |
| $Hg^{2+}$ | Dual detection system-colorimetric detection: aptamer coated poly-styrene (PS) beads; AuNP; silver nanoparticles (AgNP); electrochemical detection; paper-based microfluidic component (μ-PAD); DNA aptamer | Electrochemical detection: LOD of 0.01 ppm; dynamic range: 0.01–1 ppm (adj. $R^2 = 0.935$); colorimetric system: PS-AuNPs-based system – qualitative detection (LOD 5 ppm), stable >7 days (97.59% signal retention); PS-AgNPs-based system – LOD 0.5 ppm, linear range 0.5–20 ppm (adj. $R^2 = 0.986$), stable >30 days (94.95% signal retention) | 193 |
| $K^+$ | Microfluidic aptasensor; PMMA/paper-microchip; integrated RGB analy-sis system; AuNPs; DNA aptamer; smartphone app | Detection range of 0.05 to 9 mM ($R^2 = 0.994$), (LOD) of 0.01 mM. 137 whole blood and 287 serum samples of chronic kidney disease (CKD) patients consistent ($R^2 = 0.968$ and $R^2 = 0.980$) with ion-selective electrodes (ISE) method | 194 |
| Diacetyl | Cell-free expression system; ODR-10 receptor (protein); anti-His6-tag aptamer; electrolyte-insulator–semiconductor (EIS) sensors; capacitance–voltage (C–V) and constant-capacitance (ConCap) | LOD: 0.01 nM, dynamic range: 0.01–1 nM | 195 |
| 3,3′,4,4′-Tetrachlorobiphenyl (PCB77) | Microfluidic electro-chemical aptamer sensing platform; exonuclease I (Exo I); DNA/AuNPs/HRP nanoprobes; Au/MoS$_2$-CNTs-GO (Au/MCG) hybrids electrode | Concentration range of 0.01–1000 ng $L^{-1}$, LOD: 0.00885 ng $L^{-1}$ | 196 |
| 3,3′,4,4′-Tetrachlorobiphenyl (PCB77) | Electrochemical apta-sensor; Au/Nb$_2$CT$_x$/GO hybrids electrode; methylene blue/thiol-labeled cDNA (MB-COOH-cDNA-SH); ferrocenyl-modified aptamer (aptamer-fc) | Detection range: 0.0001 to 1000 ng $mL^{-1}$, LOD: $1.56 \times 10^{-5}$ ng $mL^{-1}$ | 197 |
| Imidacloprid, carbendazim (pesticide) | μ-PAD; PS-AuNP-aptamer-BSA; colorimetric detection; smartphone-integrated biosensor | LOD: imidacloprid (3.12 ppm), LOD: carbendazim (1.56 ppm), detection range: 0.39–100 ppm | 198 |
| Tobramycin | PDMS micro-channels integrated with rGO/Au aptamer FET; 6-mercapto-1-hexanol (MCH)/1-pyrenebutanol (PBA) blocking elemental sensing | LOD: 0.3 nM (0.14 μg $L^{-1}$), detection range: $10^{-8}$ M-$10^{-4}$ M, detection within 5 s | 199 |
| Ochratoxin A (OTA) | Lab-on-Chip (LoC) integrated aptasensor; fluorescent molecule [Ru(phen)2(dppz)]$^{2+}$, 2(hydroxylethyl methacrylate) (PHEMA) functionalized glass; aptamer | LOD: 1.3 ng $mL^{-1}$, detection range: 5–200 ng $mL^{-1}$, small sample volume (~10 μL), short time (5 min) | 200 |
| Kanamycin | Microfluidic chip-based ratiometric aptasensor with rolling circle amplification (RCA) | LOD: 0.3 pg $mL^{-1}$, detection range: 0.8 pg $mL^{-1}$ to 10 ng $mL^{-1}$, small sample volume (150 pL) | 201 |
| Ochratoxin A (OTA) | Graphene field-effect transistor (GFET) | LOD: 4 pg $mL^{-1}$, detection range: 10 pg $mL^{-1}$–4 ng $mL^{-1}$ | 202 |
| Okadaic acid | Phosphorene-gold nanocomposite-based aptasensor; screen-printed carbon electrodes (SPCE); black phosphorous (BP); BP-Au nanocom-posite (BP-Au NC) | LOD: 8 pM, linear range of detection: 10–250 nM ($R^2 = 0.9887$) | 203 |
| Kanamycin, aflatoxin M1 (AFM1), 17β-estradiol (E2) | Magnetic tripartite DNA aptasensor with microfluidic chip; RCA; phi29 polymerase | LOD: 0.32 pg $mL^{-1}$ (KANA), 0.95 pg $mL^{-1}$ (AFM1), 6.8 pg $mL^{-1}$ (E2); detection range: 0.001–100 ng $mL^{-1}$ | 204 |

**Table 6** (continued)

| Targets | Microfluidic methodology | Detection performance | Ref. |
|---|---|---|---|
| | | (KANA), 3–50 pg mL$^{-1}$ (AFM1), 0.02–2 ng mL$^{-1}$ (E2) | |
| Aflatoxin M1 | Microfluidic paper-based analytical device (μPAD); AuNP; 21-mer aptamer | LOD: 3 pM in buffer, 10 nM in milk; detection range: 1 μM–1 pM | 205 |
| Enrofloxacin (ENR) | Lateral flow strip with smartphone readout; lateral flow-based biosensor (LFB); end-regulated AuNP clustering (TAuC) | LOD: 0.1 μg L$^{-1}$, detection range: 0.1–10$^4$ μg L$^{-1}$ | 206 |
| Ochratoxin A (OTA) | Liquid crystal-based aptasensor | LOD: 0.63 aM, ultra-low detection in food and human serum samples, range: 0.001–400 fM | 207 |
| Aflatoxin-M1 | Microfluidic electro-chemical biosensor; graphene quantum dot-gold nanoparticle, GQDA | LOD: 0.397 nM, detection range: 100 pM–2 nM | 208 |
| Δ9-Tetrahydrocannabinol (THC) | Electrochemical aptasensor on a microfluidic platform | LOD: 1 nM in PBS, 10 nM in 10% diluted saliva, 5 nM in size excluded filtration pretreated saliva, rapid detection in 1 min | 209 |
| Enrofloxacin (ENR) | Localized Surface Plasmon Resonance (LSPR) sensing chip with microfluidic device; AuNP | LOD: 0.001 ng mL$^{-1}$; detection range: 0.01–100 ng mL$^{-1}$; recovery: 91.94–108.38% in real water samples | 210 |
| Ochratoxin A (OTA) | Thermal-regulated sensor integrated with covalent organic framework (COF); COF-Au-MB-Apt signal probe | LOD: 0.12 pg mL$^{-1}$, detection range: 0.2 pg mL$^{-1}$ to 0.6 μg mL$^{-1}$ | 211 |

device that detected levels as low as 3 pM in buffer and 10 nM in milk, while Ramalingam et al.[208] used a biochip with graphene quantum dot-gold nanoparticles to achieve an LOD of 0.4 nM. The same group also developed an electrochemical microfluidic biochip for okadaic acid (OA) detection using a polydimethylsiloxane (PDMS) platform and aptamer-modified screen-printed carbon electrodes.[203] In real-world shellfish samples, the sensor showed excellent selectivity and performance with 8 pM LOD and a linear detection range of 10–250 nM. Moreover, another group utilized an electrochemical aptasensor with a 3D-printed microfluidic cartridge detects Δ9-tetrahydrocannabinol (Δ9-THC) in saliva.[209] This sensor had high specificity with a LOD of 1 nM in PBS and 5 nM in saliva, making it a promising point-of-care cannabis detection tool. These works have demonstrated great potential for aptamers on microfluidics for toxin detection (Table 6).

**5.3.3 Large biomolecules.** Aptamers have been used for detection of large molecules on microfluidic systems. For instance, Ma et al.[212] developed a microfluidic electrochemical biosensor for endotoxin detection, achieving an LOD of 0.5 ng mL$^{-1}$ at a dynamic range of 0.5 to 200 ng mL$^{-1}$. Similarly, Nascetti et al.[213] developed an embedded sensor chip featuring chemiluminescence-based adenosine triphosphate (ATP) detection, with a detection limit of 60 nM and a detection range from 0.3 nM to 20 μM; Niu et al.[214] employed continuous injection-electrostacking within an IMC for lipopolysaccharide detection (LOD = 7.9 fM in water). Moreover, Nandimandalam et al.[215] used a lab-on-chip platform integrating split aptamers immobilized on polymer brushes for ATP detection with an LOD of 0.89 μM, and Weng et al.[216] presented a portable 3D microfluidic origami biosensor for cortisol detection, achieving an LOD of 6.8 ng mL$^{-1}$ at a detection range of 10 to 1000 ng mL$^{-1}$. These studies have paved a way for developing compact devices for detecting various molecules. More detail information could be found in Table 7.

## 5.4 Proteins

**5.4.1 Thrombin.** Proteins are the most-targeted molecules for detection via microfluidic platforms, and thrombin has been particularly well studied. For instance, aptamer-functionalized microparticles were used to separate thrombin, IgE, and mCardinal2 simultaneously using acoustofluidics for clinical diagnostic applications.[217] In another work, a microfluidic-integrated graphene field-effect transistor biosensor was developed to selectively and sensitively detect thrombin biomarkers at an LOD of 2.6 pM for POC diagnostics.[224] An integrated pneumatic microfluidic circuit with autonomous pumps was designed to separate plasma for rapid POC molecular diagnostics.[115] Additionally, Xue et al.[234] developed a microfluidic, paper-based photoelectrochemical sensing platform for thrombin detection using electron-transfer tunneling distance regulation and aptamer target-triggering nicking enzyme signaling amplification; this device demonstrated high sensitivity and clinical diagnostic potential (Table 7).

**5.4.2 Allergens.** All kinds of allergens have been demonstrated using aptamers on microfluidics. For instance, food safety requires detection of the peanut allergen Ara h1, a protein that causes mild skin irritation to life-threatening anaphylaxis in a large percentage of peanut-induced allergic reactions. A microfluidic origami electrochemical nano-aptasensor with black phosphorus nanosheets could detect Ara h1 across a linear range of 50–1000 ng mL$^{-1}$ and an LOD of 22 ng mL$^{-1}$ for low-cost, rapid food safety-testing.[223] Another group further developed a paper-based microfluidic device with black phosphorus-gold nanocomposites that could detect Ara h1 across a linear range of 25–800 ng mL$^{-1}$ and an LOD of 12 ng mL$^{-1}$ in food products[230] (Table 7).

**5.4.3 Proteins as infectious disease biomarkers.** Proteins could serve as valuable biomarkers for a wide range of acute and chronic diseases. For instance, one IMC employed an aptamer/antibody sandwich method to detect the COVID-19

nucleocapsid protein at a detection limit of 33 pg mL$^{-1}$ (300-fold more sensitive than enzyme-linked immunosorbent assay (ELISA)), making it ideal for early diagnosis.[222] Another group developed an IMS for screening SARS-CoV-2 S1 aptamers, achieving an LOD of 48 copies mL$^{-1}$ for the Wuhan strain and 195 copies/mL for the Omicron strain, thus enabling efficient and accurate diagnosis[42] (Table 7).

Periprosthetic joint infections (PJIs) are serious complications that can result from joint replacement surgeries and cause severe joint pain, implant failure, and the need for additional surgeries. Gondotra et al.[41] developed an IMS for selecting aptamers against alpha-defensin human neutrophil peptide 1 (HNP1), which is a biomarker for PJIs in synovial fluid with a $K_d$ of 19 nM using an ELISA-like assay. A paper-based aptamer-sandwich assay integrated into an IMS to detect HNP1 was further characterized by a detection limit of 0.5 mg L$^{-1}$ across a dynamic range of 0–100 mg L$^{-1}$, making it a rapid, cost-effective POC diagnostic tool.[221] Finally, another work introduced an IMS for selecting high-affinity aptamers targeting HNP1–3 with a detection limit of 0.3 mg L$^{-1}$ and efficient SELEX screening with minimal human intervention, thereby improving PJI diagnostics.[43] These works have demonstrated that aptamers could be used to capture protein biomarkers targeting infectious diseases (Table 7).

**5.4.4 Proteins as cardiovascular disease biomarkers.** Cardiovascular disease (CVD), the leading cause of death globally, can lead to heart attacks, strokes, and heart failure. Aptamers have been used for CVD diagnosis. For instance, Li et al.[226] developed a self-driven microfluidic, integrated-circuit biosensing microfluidic chip that detected four cardiovascular disease biomarkers, including N-terminal pro-B-type natriuretic peptide (NT-proBNP), fibrinogen, cardiac troponin I (cTnI), and C-reactive protein (CRP; an inflammation biomarker) - with low detection limits and aptamer-coated interdigitated electrodes for rapid, POC diagnostics. Another group utilized a colorimetric approach and gold-decorated microparticles to detect cTnT at a detection limit of 0.39 ng mL$^{-1}$ with a smartphone-based, paper microfluidic aptasensor for sensitive and portable acute myocardial infarction diagnosis.[233] CRP has been targeted in multiple studies using microfluidic aptasensors.[218,225,226,233,236] For instance, one article reported a micro-ring resonator-based biosensor that used optimized surface functionalization and specific aptamers to improve thrombin and CRP detection sensitivity.[218] Another acoustofluidic device used aptamer-functionalized microparticles to separate thrombin and CRP from platelets in plasma at 1.6 mL h$^{-1}$ flow rate, >95% efficiency, demonstrating its potential for multiplexed liquid biopsy applications in CVD detection[225] (Table 7).

**5.4.5 Protein as biomarkers for cancer diagnosis.** Several groups have explored the use of aptamers and microfluidic technologies for cancer biomarker detection, which is essential for early diagnosis, treatment monitoring, and patient outcomes. For instance, an electrolyte-gated organic field-effect transistor with microfluidic channels could detect tumor necrosis factor α (TNFα) at a 3 pM detection limit, improving POC diagnostics.[183] Similarly, Su et al.[232] developed a cloth-based, bipolar, solid-state, electrochemiluminescence aptasensor for carcinoembryonic antigen detection; with an LOD of 1.6 pg mL$^{-1}$, this durable, cost-effective device is also suitable for POC applications. Additionally, an IMC enabling dielectrophoretic separation and differential pulse voltammetry rapidly detected prostate-specific antigen (PSA) in blood at 0.25 pg mL$^{-1}$.[184] Another group[235] devised an IMS combining flow cytometry and mass spectrometry for high-throughput biomarker and drug uptake profiling in single cells, enabling personalized cancer treatment and therapeutic monitoring. It is a growing trend to use aptamers on microfluidics for cancer biomarker detection (Table 7).

**5.4.6 Other proteins.** Microfluidic platforms have demonstrated versatility in detecting diverse protein targets. For instance, a 3D-printed, polyacrylate-based system with optical, nano-structured, porous silicon enhanced biosensing of arabinanase D2, reducing sample volumes and improving sensitivity (0.25 to 18 μM) over other PDMS-based methods[219] and could be used in medical diagnostics and environmental monitoring.[219] Alternatively, a lab-on-chip platform used PCR-amplified DNA aptamers to quantify leptin more rapidly (~2 h) and sensitively (LOD = 100 pg mL$^{-1}$) than ELISA.[220] Moreover, an internet of things (IoT)-based aptasensor biochip was developed to detect the periodontal disease biomarker odontogenic ameloblast-associated protein (ODAM).[228] Alternatively, a sandwich-type fluorescence aptasensor using an aptamer pair (MB-OD64 & FAM-OD35) selectively bound target ODAM within 30 min at an LOD of 0.01 nM (Table 7).

Another study introduced an organic electrolyte-gated field-effect transistor (FET) with microfluidic channels for non-invasive α-synuclein detection in saliva.[227] The detection limit was 10 fg L$^{-1}$, demonstrating potential for early Parkinson's disease diagnosis. Ogunmolasuyi et al.[229] developed a microfluidic paper analytical device to rapidly detect Plasmodium falciparum lactate dehydrogenase, offering low-cost malaria diagnosis.[229] Another microfluidic electrochemical aptasensor was integrated into a polydimethylsiloxane (PDMS)-based flexible microfluidic device with a MoS$_2$/graphene/gold nanocomposite-modified electrode for detection of gliadin at an LOD of 7 pM within 20 min at a detection range of 4–250 nM.[231] These specifications make it suitable for POC food safety assessments, notably in identifying gluten-free foods. Moreover, a microfluidic, dual-aptamer sandwich assay for rapid detection of His-tagged recombinant proteins[88] screened aptamers for His-tag and IgE via microfluidic SELEX and was associated with an LOD of 7.1 nM within 10 min.[88] The aptamer surfaces were reusable for up to 20 cycles, maintaining consistent performance; this could lead to reduced costs (Table 7).

## 5.5 Virus and exosomes/extracellular vesicle (EV) targets

**5.5.1 Viruses.** Several studies have advanced viral detection using microfluidic and biosensing technologies via aptamers. For instance, a study[237] developed a microfluidic chip for

**Table 7** List of research works using aptamers targeting biomolecules to proteins

| Targets | Microfluidic methodology | Detection performance | Ref. |
|---|---|---|---|
| Endotoxin | Microfluidic electro-chemical biosensor; electrochemical impe-dance spectroscopy (EIS); aptamer/AuNP/SPCE | LOD: 0.5 ng mL$^{-1}$, detection range: 0.5 to 200 ng mL$^{-1}$ | 212 |
| Adenosine triphosphate (ATP) | PLEIADES chip with chemiluminescence detection; combine of an autonomous capillary force-driven microfluidic network; an array of thin-film hydrogenated amorphous silicon photosensors, and chemiluminescence bioassays | With immunoassay for ATP: LOD: 60 nM, detection range: 0.3 nM to 20 µM; demonstrated feasibility of combining aptamer nanoswitch | 213 |
| Lipopolysaccharide (LPS) | Continuous injection-electrostacking (CI-ES) biochip | LOD: 7.9 fM (water), 8.3 fM (serum), detection range: 50 fM–10$^6$ fM in water, 50–10$^4$ fM in serum | 214 |
| ATP | Lab-on-chip with PHEMA-aptamer fragments; amorphous silicon (a-Si:H) photosensor; polyhydroxyethyl-methacrylate (PHEMA); [Ru(phen)2(dppz)]$^{2+}$ light switch | LOD: 0.89–0.98 µM, detection range: 0.1–1000 µM | 215 |
| Cortisol | 3D microfluidic origami biosensor; molybdenum disulfide (MoS$_2$) nanosheet-mediated fluorescence resonance energy transfer (FRET); fluorescently labeled aptamers | LOD: 6.76 ng mL$^{-1}$, detection range: 10–1000 ng mL$^{-1}$ | 216 |
| Thrombin, immunoglobulin E (IgE) | Acoustofluidic separation using traveling surface acoustic waves (TSAW) | Separation efficiency: 99.04% for thrombin, 98.85% for IgE; recovery rate: 97.82% for thrombin, 96.31% for IgE | 217 |
| C-reactive protein, thrombin | Microring resonator (MRR)-based biosensor with aptamer-functionalization | Best condition for MRR surface immobilization of aptamer: argon plasma, 1% v/v mercaptosilane, concentration and time optimized 1 µM and 3 h | 218 |
| His-tagged proteins (D2 protein in arabinanase family) | 3D-printed polyacrylate microfluidic device integrated with porous silicon (PSi) aptasensors | Detection range: 0.25–18 µM, LOD: 0.04 µM, LOQ: 0.16 µM, RSD 12–22% | 219 |
| Leptin | PCR amplification of short DNA aptamers in a lab-on-chip implementation | LOD: 100 pg mL$^{-1}$ for leptin, significant reduction in assay time to less than 2 hours | 220 |
| Alpha-defensin human neutrophil peptide 1 (HNP1) | Integrated microfluidic system for aptamer selection | Aptamer selected: $K_d$ 19 nM, LOD: 0.1 mg L$^{-1}$, dynamic range: 0.1–100 mg L$^{-1}$ | 41 |
| Human neutrophil peptide 1 (HNP1) | Paper-based aptamer-sandwich assay | Detection limit (LOD): 0.5 mg L$^{-1}$; dynamic range: 0.5–100 mg L$^{-1}$ | 221 |
| Alpha-defensin human neutrophil peptide 1–3 (HNP1–3) | Integrated microfluidic platform for diagnostic assays | LOD: 0.3 mg L$^{-1}$, dynamic range: 0.32–100 mg L$^{-1}$, sample volume 50 µL, assay time <3 hours | 43 |
| SARS-CoV-2 nucleocapsid protein | Aptamer/antibody sandwich method on a microfluidic chip | LOD: 33.28 pg mL$^{-1}$, 100 pg mL$^{-1}$ to 100 ng mL$^{-1}$ | 222 |
| Peanut allergen Ara h1 | Microfluidic origami electrochemical nano-aptasensor, black phosphorus nanosheets, BPNSs | LOD: 21.6 ng mL$^{-1}$; linear range: 50–1000 ng mL$^{-1}$, detection time 20 minutes, sensitivity: 0.05 µA·ng mL$^{-1}$; recovery rate: 98.3–107.9% in spiked cookie dough samples; relative standard deviation (RSD) < 5% | 223 |
| Thrombin biomarker | Integrated microfluidic platform with graphene FET biosensor | LOD: 2.6 pM for thrombin; dissociation constant $K_d$ = 375.8 ± 165.6 pM, selectivity tested against lysozyme | 224 |
| Thrombin, C-reactive protein (CRP) | Acoustofluidic separation using aptamer-functionalized micro-particles, surface acoustic waves (SAW); interdigital transducer (IDT) | Separation efficiency >95%, flow rate 1.6 ml h$^{-1}$, maximum flow velocity: 37.04 mm s$^{-1}$; LOD not explicitly stated | 225 |
| NT-proBNP, fibrinogen, cTnI, CRP | Self-driven, microfluidic integrated-circuit (IC)-based biosensing chip with aptamer-coated interdigitated electrodes (IDE) | LOD: NT-proBNP: 1.53 pg mL$^{-1}$, fibrinogen: 59.4 mg dL$^{-1}$, cTnI: 0.54 pg mL$^{-1}$, CRP: 0.39 mg L$^{-1}$; dynamic ranges: NT-proBNP (0.1–10 000 pg mL$^{-1}$), fibrinogen (50–1000 mg dL$^{-1}$), cTnI (0.1–10 000 pg mL$^{-1}$), and CRP (0.5–9 mg L$^{-1}$), total 15 min detection time | 226 |
| α-Synuclein (αSyn) in saliva, Parkinson's disease (PD) patient | Organic electrolyte-gated field-effect transistor (OEGFET) with soft microfluidics | LOD: 10 fg L$^{-1}$; $K_d$: 10 ng L$^{-1}$ (6.6 pM), linear range: 100 fg to 10 µg L$^{-1}$, recovery rate: 88.6% to 104%; repeatability over a month | 227 |
| Odontogenic ameloblast-associated protein (ODAM) | IoT-based microfluidic point-of-care (POC) biosensing chip with aptamer-based sandwich-type binding | LOD: 0.011 nM (~0.36 ng mL$^{-1}$); detection time: 30 min; specificity: 100% for ODAM detection; linear range: 0.15–6.25 nM | 228 |
| Plasmodium falciparum LDH (PfLDH) | Microfluidic paper analytical device (µPAD) with aptamer-based detection | LOD: 17 nM, $K_d$: 24 ± 11 nM in buffer, specific recognition of 133 nM rPfLDH in serum and blood samples | 229 |
| Peanut allergen Ara h1 | Paper-based microfluidic device with BP-Au nanocomposites for signal amplification; µ-PAD | LOD: 11.8 ng mL$^{-1}$; linear range: 25–800 ng mL$^{-1}$; analysis time: 20 min; recovery rate: 93.50%–101.86% with RSDs of 0.36%–2.97% ($n$ = 3) | 230 |

**Table 7** (continued)

| Targets | Microfluidic methodology | Detection performance | Ref. |
|---|---|---|---|
| Tumor necrosis factor alpha (TNFα) | Lab-on-chip multigate organic transistor (EGOFET); peptide affimer | LOD: 3 pM; dynamic range: 0.1–1000 pM | 183 |
| Gliadin | Electrochemical microfluidic biochip with MoS$_2$/graphene/Au nanocomposite | LOD: 7 pM, linear detection range: 4–250 nM ($R^2$ = 0.982), total assay time: 20 min | 231 |
| Thrombin | Integrated microfluidic pneumatic circuit (iPC) for point-of-care diagnostics | LOD: 133.37 pM, detection range: up to 600 pM | 115 |
| Carcinoembryonic antigen (CEA) | Cloth-based closed bipolar solid-state electrochemiluminescence (CBP-SS-ECL) aptasensor | LOD: 1.6 pg mL$^{-1}$; linear range: 5–100 000 pg mL$^{-1}$ | 232 |
| Cardiac troponin T (cTnT) | Smartphone-based paper microfluidic aptasensor with colorimetric detection; μ-PAD | LOD: 0.39 ng mL$^{-1}$; linear ranges: 0.01–0.8 μg mL$^{-1}$ and 6.25–50 μg mL$^{-1}$, platform stable >23 days | 233 |
| Prostate-specific antigen (PSA) | Microfluidic chip integrated with dielectrophoretic (DEP) separation and differential pulse voltammetry (DPV) detection | LOD: 0.25 pg mL$^{-1}$; linear range: 1 pg mL$^{-1}$–10 ng mL$^{-1}$, good stability to 15 days at 4 °C | 184 |
| His-tagged recombinant proteins, his-IgE | Microfluidic dual-aptamer sandwich assay | LOD: 7.1 nM; detection time: 10 min in culture media; dual-aptamer approach enhanced sensitivity and reusability | 88 |
| SARS-CoV-2 S1 protein | Automatic integrated microfluidic system for aptamer screening | LOD: 48 copies per mL (Wuhan strain); LOD: 195 copies per mL (omicron strain); affinity ($K_d$): 63 nM | 42 |
| Thrombin | Microfluidic paper-based photoelectrochemical sensing platform, μ-PEC; electron-transfer tunneling distance regulation (ETTDR); nicking enzyme signaling amplification (NESA) | LOD: 6.7 fM, detection range: 0.02 pM to 100 pM | 234 |
| Biomarker and drug uptake in single cells, protein tyrosine kinase 7 (PTK7) protein on cancer cells | Microfluidic flow cytometry with mass spectrometry (μCytoMS), 6-FAM-Sgc8 aptamer functionalized AuNP | $K_d$: 0.23 nM for PTK7 detection; throughput: 500 cells per min; single-cell drug uptake analysis using oxaliplatin (OXA) | 235 |

selective isolation of active SARS-CoV-2 virus particles, using surface-bound aptamers targeting the spike protein's receptor-binding domain. The chip design included 1.5 million diamond-shaped micropillars, optimizing surface area for efficient virus capture. The system achieved 94% recovery of virus particles, with 89% release efficiency using blue light. In clinical trials, the device demonstrated a 95% sensitivity and relatively high specificity for detecting active SARS-CoV-2, distinguishing patients with active disease from those with non-active viral fragments. Another strategy used a microfluidic enrichment system based on stoichiometric balanced DNA computation, utilizing dual-domain aptamers targeting different spike protein regions and cholesterol-DNA for viral envelope interaction.[238] This herringbone microfluidic chip enhanced viral particle capture by inducing chaotic flow and thus improving interactions and demonstrated an LOD of 37 active virions μL$^{-1}$ and a 90% release efficiency of intact SARS-CoV-2 particles *via* DNase I treatment, enabling high-throughput viral culture and downstream analysis. Moreover, a microfluidic device with aptamer-functionalized gold nanoparticles detected Zika and Chikungunya viral envelope proteins at 1 pM in PBS and 100 pM in calf blood.[239] Similarly, an on-chip integrated graphene aptasensor detected SARS-CoV-2 particles and neutralizing antibodies at 10$^3$ particles per mL and 160 aM, respectively, for POC diagnostics.[240] These studies demonstrate the effectiveness of microfluidic biosensing technologies employing aptamers for high-specificity/high-sensitivity viral detection (Table 8).

**5.5.2 Exosomes and EVs.** Exosomes are EVs measuring 30–150 nm that play crucial roles in intercellular communication and disease pathogenesis.[262,263] Their presence in bodily fluids and potential as biomarkers make them attractive for clinical applications,[264] and microfluidic technologies can significantly enhance the isolation and detection of exosomes and EVs *via* aptamers. For example, Bai *et al.*[241] employed Dean-flow coupled elasto-inertial microfluidics to separate exosomes from proteins in biological fluids, utilizing spiral microchannels and viscoelastic lift forces to enhance separation by using aptamers. The system achieved 71% recovery of exosomes with 91% removal of protein contaminants, enabling single-vesicle profiling for downstream analyses. Another report by Chen *et al.*[242] introduced a microfluidic device with a micro-column array for isolating exosomes and simultaneously detecting surface proteins and miRNAs using a catalytic hairpin assembly signal amplification strategy composed by aptamers. It achieved an LOD of 83 exosomes per μL, allowing for the distinction of different cancer subtypes, as well as cancer patients from healthy individuals (Table 8).

Moreover, Chinnappan *et al.*[243] utilized an aptamer-magnetic microfluidic platform for isolating and detecting colorectal cancer exosomes, with anti-CD63 aptamers conjugated to magnetic nanobeads used for recognition. This platform achieved a detection limit of 1457 particles per mL and high specificity against closely related proteins, showing potential for rapid exosome isolation and cancer biomarker

**Table 8** List of research works using aptamers virus, exosome/EVs, and bacteria

| Targets | Microfluidic methodology | Detection performance | Ref. |
|---|---|---|---|
| Active SARS-CoV-2 virus particles | Microfluidic chip with surface-bound aptamers and blue-light release | Recovery: 94%; release efficiency: 89%; sensitivity: 95% (for 19 out of 20 COVID-19 positive patients) | 237 |
| Intact SARS-CoV-2 particles | Microfluidic enrichment with stoichiometric balanced DNA computation, AND logic gate, cholesterol-DNA, dual spike protein aptamer | LOD: 37 virions per µL, viral release efficiency: 90%; sensitivity: 100% for 14 COVID-19 patients, specificity: 100% | 238 |
| Zika and Chikungunya virus proteins | Polydimethylsiloxane-based microfluidic device with gold nanoparticle (AuNP) aptamers | LOD: 1 pM (50 pg mL$^{-1}$) (Zika); sensitivity: 100 pM in calf blood; 10 pM in dilute (10%) mechanically defibrinated calf blood | 239 |
| SARS-CoV-2 particles, antibodies | On-chip integrated graphene field-effect transistor (GFET) aptasensor, aptamer-functionalized GFET (aptasensor, Apt-GFET) | LOD: $10^3$ particles per mL; 160 aM for neutralizing antibodies | 240 |
| Exosomes from human serum and cell culture | Dean-flow-coupled elasto-inertial focusing (DEIC), spiral microchannel with dimensional confined concave structures | Recovery rate: 70.6%; protein removal rate: 91.4%; single-vesicle-level biomarker profiling using aptamers for EpCAM and PD-L1 | 241 |
| Non-small cell lung cancer (NSCLC)-related exosomes | Ship-shaped microfluidic device with PDMS microcolumn array, CD63 protein aptamer, catalytic hairpin assembly (CHA) | LOD: 83 exosomes per µL; linearity range: $10^4$–$10^9$ exosomes per mL; multiplex detection of EpCAM, EGFR, miRNA-21, and miRNA-200, distinguishing cancer cell subtypes and lung cancer patients | 242 |
| Colorectal cancer exosomes | Aptamer-magnetic biosensor with transverse magnetic field, rotating magnet assembly system (rMAS) | LOD: 1457 particles per mL; linear range: $1.75 \times 10^3$ to $8.75 \times 10^7$ particles per mL; specificity tested with closely related proteins; aptamer-magnetic bead method for isolation and pre-concentration | 243 |
| Exosomal miRNA-210 (cancer biomarker) | Microfluidic aptamer-conjugated magnetic nanobeads for separation | LOD: 5 pM (miRNA-210); linear range: 0.05–100 nM; fluorescence-based detection with carbon nanomaterial-coated magnetic beads | 244 |
| Exosomal membrane proteins (PD-L1, EpCAM, CA125) | Centrifugal microfluidic disc and aptamer-based fluorescence detection, automated centrifugal microfluidic disc system (Exo-CMDS), aptamer fluorescence system (Exo-AFS) | LOD: $1.58 \times 10^5$ particles per mL for PD-L1, exosome yield: $5.1 \times 10^9$ particles per mL in 8 minutes; diagnostic accuracy: 91% for lung cancer | 245 |
| Cancer-associated exosomes | Drop-shaped micropillar microfluidic chip, cationic perylene tetracarboxylic acid diimide derivative (PTCDI), aptamers targeting CD63, PD-L1, CA125, nucleolin, EpCAM, PTK-7, PSMA | LOD: $8.69 \times 10^3$ particles per mL, detection range: $8.74 \times 10^3$ to $1.37 \times 10^8$ particles per mL | 246 |
| Exosomes carrying CD63 and PTK7 | Aptamer-based microfluidics system with surface-modified channels | Capture efficiency: $10^7$–$10^8$ particles per mL in 20 min, specific isolation of exosomes based on CD63 and PTK7 aptamers | 247 |
| Extracellular vesicles (EVs) | Integrated ExoID-Chip with photonic crystal nanostructure, aptamer targeting CD63 | LOD: $8.9 \times 10^3$ EVs mL$^{-1}$; sample volume: 20 µL; successfully distinguishes breast cancer patients from healthy controls | 248 |
| PD-L1 EV subpopulations (tumor and non-tumor origin) | DNA computation mediated microfluidic tandem separation | LOD: 4.79 pg mL$^{-1}$ for PD-L1; selective isolation of tumor and non-tumor PD-L1 EVs | 249 |
| *Escherichia coli* (E. coli) | Non-faradaic impedance biosensor, IDE arrays, OMP Ag1 aptamer targeting *E. coli* | LOD: 9 CFU mL$^{-1}$; sensitivity: 1.8 ohm CFU$^{-1}$; analytical range: 25–1000 CFU mL$^{-1}$ | 250 |
| *E. coli* O157:H7 | Dendrimer-aptamer modified PDMS microfluidic channels | LOD: $10^2$ CFU mL$^{-1}$ in G7 channels, comparison between G7 and G4 dendrimers showed higher detection efficiency for G7-modified surfaces | 182 |
| *Streptococcus pneumoniae* | Aptamer decorated PDA@magnetic silica microparticles, SELEX | Capture efficiency: 87% in PBS, 66% in blood, aptamer affinity: $K_d = 72.8$ nM | 251 |
| *Campylobacter jejuni*, *Aliarcobacter butzleri* | Fusarinine C-magnetic nanoparticles and aptamer-red/-green carbon dots | LOD: 1 CFU mL$^{-1}$ for each bacterium, detection range up to $1 \times 10^7$ CFU mL$^{-1}$; RGB color detection enabled detection with LOD of 5 CFU mL$^{-1}$ in 65 min | 252 |
| *Salmonella typhimurium* | Colorimetric biosensor, smartphone APP, thiolated microspheres | LOD: $6.0 \times 10^1$ CFU mL$^{-1}$, detection time: 45 minutes; recovery in salad samples: 91.68–113.76% | 253 |
| *Bacillus subtilis* in soil | Toggle-cell SELEX, portable aptamer-based detection technology with magnetic beads | $K_d$: 23.74 ± 1.19 nM; $B_{max}$: 3.24 ± 0.16 nM; detection in soils with inoculated *B. subtilis*: $3.67 \times 10^6$ to $3.37 \times 10^7$ cells per mL | 254 |
| *Salmonella typhimurium* | Digital PCR Chip with aptamer-coated magnetic beads | Detection as low as 90 CFU per reaction, with a capture efficiency of 94.5%. The process takes about 2 hours | 255 |
| *Helicobacter pylori* | Superparamagnetic nanoparticles with fluorescence-based detection | Detection range of 10–$10^7$ CFU mL$^{-1}$ with an LOD of 1 CFU mL$^{-1}$, Total detection time: 65 minutes | 256 |
| *Acinetobacter baumannii* | Nitrocellulose membrane-based microfluidic system with electromagnetic micro-devices | Detection limit as low as 450 CFU per reaction within 40 minutes | 257 |
| *Vibrio parahaemolyticus* | Capillary microfluidic chip with magnetic beads manipulation | Complete detection in 40 minutes with high selectivity using capillary force | 258 |
| *Bacillus cereus* | Portable dual-aptamer microfluidic chip biosensor, | On bench assay: LOD: 4.85 CFU mL$^{-1}$, detection range: | 259 |

**Table 8** (continued)

| Targets | Microfluidic methodology | Detection performance | Ref. |
|---|---|---|---|
| | rolling circle amplification (RCA) method | $1.15 \times 10^1$ to $1.15 \times 10^6$ CFU mL$^{-1}$, portable microfluidic chip: LOD: 9.27 CFU mL$^{-1}$, detection range: $1.59 \times 10^2$– $1.59 \times 10^7$ CFU mL$^{-1}$ | |
| E. coli O157:H7 | Tetrahedral DNA nano-structure (TDN)-aptasensing microcavity, nano-bio aptasensing interface, integrated microfluidic chip, framework nucleic acids (FNAs) | LOD: 10 CFU mL$^{-1}$, enrichment efficiency: Enhanced with TDN-engineered microchannel | 260 |
| Pseudomonas aeruginosa | PDMS-paper hybrid microfluidic chip | LOD: 10 CFU mL$^{-1}$, detection time: 15–20 minutes, linear detection range: 10 CFU mL$^{-1}$ to 1000 CFU mL$^{-1}$ | 261 |

detection in clinical applications.[243] Another study demonstrated a microfluidic device using aptamer for the isolation and detection of exosomal Mir-210 using carbon nanomaterial-coated MBs[244] with a fluorescence-based switching assay. The system was characterized by a detection limit of 5 pM, showing no cross-reactivity with other miRNAs; it therefore could serve as a minimally invasive method for cancer biomarker detection (Table 8).

Furthermore, Zhao et al.[245] reported the development of an automated centrifugal microfluidic disc system for exosome isolation, paired with an aptamer fluorescence system for detecting exosomal surface proteins. The system isolated $5 \times 10^9$ particles per mL in just 8 min and achieved an LOD of $1.6 \times 10^5$ exosomes mL, offering 91% diagnostic accuracy for lung cancer. Alternatively, Zheng et al.[246] demonstrated a microfluidic chip with alternating drop-shaped micropillars for efficient exosome capture using Tim4-modified MBs. The system using aptamer as signal probe achieved a detection limit of $8.7 \times 10^3$ particles/mL, enabling detailed profiling of exosomal surface proteins for distinguishing liver cancer patients from healthy individuals. Moreover, Zhou et al.[247] presented an aptamer-functionalized microfluidic system for isolating exosomes based on CD63 and PTK7 markers, achieving a capture efficiency of $10^7$–$10^8$ particles/mL in just 20 min; these specifications make it suitable for cancer diagnostics (Table 8).

Besides, Dong et al.[248] developed the ExoID-Chip, which integrated nanofiltration and photonic crystals for exosome isolation via CD63 aptamer and quantification, achieving an LOD of $8.9 \times 10^3$ EVs mL$^{-1}$ in a 20-μL sample volume. This method distinguished serum samples from breast cancer patients and healthy donors with high sensitivity. Alternatively, Lu et al.[249] introduced a DNA computation-mediated microfluidic tandem separation platform for isolating PD-L1-positive EV sub-populations via dual-aptamer recognition. The platform achieved highly efficient sequential isolation, providing insights into immuno-heterogeneity and enabling downstream proteomic analysis with high specificity and efficiency. In summary, sensitive, non-invasive, and high-throughput detection of both exosomes and EVs are now realized on novel IMC using aptamers (Table 8).

## 5.6 Bacteria and mammalian cells

**5.6.1 Bacteria.** Aptamers and microfluidic-based technologies can rapidly detect bacteria. For instance, Abdelrasoul et al.[250]

developed a non-faradaic impedance biosensor functionalized with DNA aptamers targeting E. coli, utilizing interdigitated electrodes. The biosensor demonstrated an LOD of 9 CFU mL$^{-1}$, and the system's performance showed a linear range from 25 to 1000 CFU mL$^{-1}$, offering high sensitivity and selectivity for bacterial detection. Similarly, Hao et al.[182] developed an IMS functionalized with poamidoamine dendrimers conjugated with aptamers for enhanced E. coli O157:H7 detection. The system achieved an LOD of 100 CFU mL$^{-1}$, with the generation 7 dendrimer channels providing better performance compared to generation 4 dendrimer channels due to more aptamer binding sites. Furthermore, Kavruk et al.[251] introduced aptamer-decorated magnetic silica microparticles in a microfluidic platform for purifying S. pneumoniae. The system achieved a capture efficiency of 87% in phosphate buffered saline (PBS) and 66% in blood, demonstrating high specificity and effectiveness in complex matrices (Table 8).

Furthermore, Liu et al.[252] developed a dual-channel fluorescent biosensor using aptamer-functionalized carbon dots to detect Campylobacter and Aliarcobacter. The system exhibited an LOD of 1 CFU mL$^{-1}$ and RGB color detection achieved a detection limit of 5 CFU mL$^{-1}$ within 65 min when integrated into an IMS.[252] Additionally, Man et al.[253] introduced a microfluidic colorimetric biosensor using gold nanoparticles and aptamer linked thiolated polystyrene microspheres to detect Salmonella in fresh vegetables. The platform had an LOD of 60 CFU mL$^{-1}$, with recovery rates between 92 and 114%, making it highly effective for food analysis. In addition, Manfredini et al.[254] utilized aptamers for detecting Bacillus subtilis in soil, utilizing a toggle-cell SELEX method for aptamer selection. The aptamers showed strong binding affinity with a $K_d$ in the nM-range, allowing for effective monitoring of bioinoculants in diverse soil environments[254] (Table 8).

Moreover, Suo et al.[255] developed an aptamer-coated MB-based IMC with digital PCR for the detection of Salmonella typhimurium that achieved an LOD of 90 CFU per reaction with a capture efficiency of 95% in ~2 h.[255] Similarly, Wang et al.[256] designed a biosensor using aptamer-functionalized superparamagnetic nanoparticles coupled with carbon dots to detect Helicobacter pylori. This system demonstrated a detection range of 10–$10^7$ CFU mL$^{-1}$ at an LOD of 1 CFU mL$^{-1}$.[256] Alternatively, Wu et al.[257] utilized a nitrocellulose membrane-based microfluidic system with magnetic-composite membranes for detecting Acinetobacter baumannii

by using specific aptamer, achieving an LOD of 450 CFU per reaction in 40 min. Zhang *et al.*[258] introduced a capillary microfluidic chip with aptamer-modified MBs manipulated by an external magnetic field for efficiently capturing *Vibrio parahaemolyticus* within 40 min, and Zhou *et al.*[259] developed a portable dual-aptamer microfluidic chip for the detection of *Bacillus cereus* in 1 h at an LOD of 9 CFU mL$^{-1}$. Zhu *et al.*[260] presented a tetrahedral DNA framework-engineered aptasensing microfluidic system for rapidly detecting *E. coli* O157, achieving an LOD of 10 CFU mL$^{-1}$. Finally, Zhu *et al.*[261] designed a pump-free paper/ PDMS hybrid microfluidic chip for bacteria enrichment *via* aptamer and detection, demonstrating an LOD of 10 CFU mL$^{-1}$ across a detection range of 10–1000 CFU mL$^{-1}$ in <20 min. These studies demonstrate that even low concentrations of bacteria can be detected using aptamer- and microfluidics-based technologies in near-real-time (Table 8).

**5.6.2 CTCs.** CTCs are rare cancer cells shed from tumors into the bloodstream and hold potential for cancer diagnosis and monitoring.[265,266] The primary challenge in CTC detection is their low concentration: 1–10 CTCs mL$^{-1}$ of blood in metastatic patients.[265] Aptamers show promise in isolating CTCs,[267] though obstacles persist, including CTC heterogeneity, viability concerns, and the need for improved sensitivity and specificity.[268,269] Recent research on microfluidic systems for CTC capture has advanced. For instance, one study isolated CTCs from biological fluids with 80% efficiency using EpCAM alongside vimentin monoclonal antibodies and Fc6 aptamers.[270] Hepatocellular carcinoma CTCs were captured 84% efficiently at 95% purity using a SERS-aptamer chip.[271] Using magnetic nanoparticles functionalized with MUC1 aptamers isolated CTCs with comparable efficiency to commercial kit in clinical samples.[272] An aptamer-cocktail (EpCAM + vimentin + EGFR + CD44) nano-microfluidic chip captured 71–83% of breast cancer CTCs.[273] Another group employed a deterministic lateral displacement (DLD) micropillar array integrated with a the multimarker aptamer cocktail DNA nanostructures (TP-multi-marker) DNA nanostructure on an IMC to enhance CTC capture.[274] The TP-multi-marker chip achieved 90% capture efficiency for MDA-MB-231 cells (& >90% for MCF-7 cells), outperforming the TP-3 EpCAMs and aptamer chips.[274] In blood the TP-multi-marker chip maintained efficiencies >90%, with minimal nonspecific white blood cell binding (0.04%). These methods show how microfluidic + aptamer-based systems can improve CTC detection[274] (Table 9).

A hybrid device featuring aptamer-functionalized diatom frustules recovered 95% and purified 90% of HepG2-derived CTCs,[278] while a cubic DNA nanostructure-programmed interface enhanced multivalent aptamer on isolating CTCs.[280] Multivalent CTC capture and release have been achieved with a tetrahedral DNA framework, combining aptamer-triggered hybridization chain reaction (apt-HCR) for sensing.[285] Another fluidic multivalent membrane

nanointerface with aptamer-functionalized leukocyte membrane nanovesicles improved CTC enrichment and recovery.[286] poly lactic-*co*-glycolic acid (PLGA) nanofiber devices with dual-EpCAM and N-cadherin aptamers captured 91 and 89% of A2780 and OVCAR-3 cells, respectively.[287] Additionally, dual-multivalent aptamer-conjugated nanoprobes captured single CTCs with high specificity.[289] In conclusion, CTCs are now readily isolated by microfluidic technologies *via* aptamers (Table 9).

**5.6.3 Lung cancer cells.** Microfluidic cancer detection has advanced lung carcinoma and adenocarcinoma cell diagnostics. For instance, a microfluidic electrochemical aptasensor detected A549 cells with a sensitivity of 14 cells per mL using Integrin α6β4-specific DNA Aptamer (IDA) aptamers targeting integrin α6β4.[276] Another platform with aptamer-functionalized self-assembled monolayers bound lung adenocarcinoma cells at >90%.[279] Immunomagnetic separation in serpentine microchannels with aptamer-conjugated MBs captured 70% of adenocarcinoma cells[282] and 78% of A549 lung carcinoma cells in a microfluidic channel.[284] These studies demonstrate that microfluidic methods using aptamers are capable of lung cancer cell detection (Table 9).

**5.6.4 Other cancer cells.** Magnetic spatial confinement effectively detected MCF-7 and *E. coli* O157 using aptamer-functionalized MBs.[275] A dynamically deformable microfilter functionalized with aptamer was developed for selective separation by adjusting pore size under hydrodynamic forces.[277] Using 4.5 μm aptamer modified MBs, 88% of lung cancer cells were captured.[281] A dielectrophoresis-based platform using aptamer-functionalized gold nanoparticles demonstrated high cancer cell capture efficiency,[283] while a thermo-chemo-mechanical hydrogel system efficiently sorted leukemia cells.[288] These studies demonstrate that diverse microfluidic methods are capable of cancer cell sensing (Table 9).

## 5.7 More complex objects

Developments in microfluidic systems have demonstrated the versatility and therapeutic potential of aptamer-based approaches. For instance, a recent study found that aptamer-modified gold nanoshells improved photothermal therapy efficiency, reducing 3D tumor spheroid viability by up to 69%.[148] An aptamer based electrochemical microfluidic biosensor with gold nano-/micro-islands detected *Cryptosporidium parvum* at only 5 oocysts per mL in buffer and 10 oocysts per mL in stool/water.[290] Furthermore, a bone-on-a-chip platform[291] revealed the protective effects of TNF-α DNA aptamers on endothelial cells against glucocorticoid-induced damage in an osteonecrosis model. Microfluidic organ-on-chip platforms have also highlighted the versatility of aptamers in developing personalized medicine, modeling complex systems, and testing therapeutic agents[50,292] (Table 9).

**Table 9**   List of research works using aptamers cells and more complex objects

| Targets | Microfluidic methodology | Detection performance | Ref. |
|---|---|---|---|
| Cancer cell, CTCs | Microfluidic Chip, AuNP, monoclonal antibody-aptamer conjugation; AuNP-Fc6-mAb | $K_d$ for AuNP-Apt-mAb: ~0.17 nM, better affinity than conjugated with either Apt or mAb; capture efficiency using AuNP-Apt-mAb was significantly higher than the other conjugates. Capture efficiency: 80% from clinical samples | 270 |
| MCF-7 and *Escherichia coli* O157 | Magnetic spatial confinement microfluidic strategy; microfluidic magnetic cell immunoassays (μMCI) | LOD: 2 cells per mL (MCF-7), 34 CFU mL$^{-1}$ (*E. coli* O157); satisfactory selectivity and reproducibility | 275 |
| Cancer cell, hepatocellular carcinoma (HCC), CTCs | Surface-enhanced Raman scattering (SERS)-aptamer based microfluidic chip | Capture efficiency: 84%, purity: 95% | 271 |
| Cancer cell, MCF-7, MDA-MB-231, HUVEC, CAF | Aptamer-targeted magnetic nanoparticles | Capture efficiency: comparable to commercial kit for clinical samples; capture efficiency >91% after 60 min when added 50 mg mL$^{-1}$ Apt-MNPs with 10 to 10$^6$ cancer cells | 272 |
| A549 cells – captured by IDA aptamer (integrin α6β4) | Microfluidic electrochemical aptasensor | LOD: 14 cells per mL, dynamic range: 50–5 × 10$^5$ cells per mL, sensitivity for A549 cells | 276 |
| Cancer cell, specific substances | Dynamically deformable microfilter | High selective separation with dynamic deformation; elastic deformation of 40 to 820 μm at flow rates of 5–40 ml min$^{-1}$; precise size-selective capture | 277 |
| Cancer cell, CTCs, breast cancer | Aptamer-cocktail functionalized nano-microfluidic chip | Capture efficiency: 71–83% for CTCs; 100% detection rate in breast cancer patients; CTC detection range of 6–33 cells per 2 ml of blood | 273 |
| Cancer cell, CTC, breast cancer | Heterovalent DNA framework recognition element-functionalized microfluidic chip; deterministic lateral displacement (DLD) pattern | Improved capture efficiency (>80%) of CTCs through deterministic lateral displacement and multimarker aptamer-based synergy | 274 |
| HepG2-derived CTCs | Hybrid microfluidic device with passive viscoelastic and active magnetophoretic separation; device with aptamer-functionalized diatom frustules | CTC recovery rate: 94.6%, purity: 89.7% | 278 |
| Human lung adenocarcinoma cells | Microfluidic platform with aptamer-functionalized self-assembled monolayer (SAM) | Cell binding coefficient: >90%; capture efficiency not directly quantified; selective capture of A549 cells confirmed | 279 |
| Circulating tumor cells (CTCs) | DNA-programmed orientation-ordered multivalent microfluidic interface; cubic DNA nanostructure (CDN)-programmed strategy to precisely control the orientation and valency of the aptamer on a microfluidic interface (CDN-Apt-Chip) | High selectivity for CTCs; enhanced capture efficiency (>80%) with CDN-Apt: binding affinity improved; successfully isolated CTCs from patient blood | 280 |
| Lung cancer cells (A549) | Immunomagnetic separation with varying magnetic bead size; serpentine microchannel with added cavities (SMAC) structure | Effective capture rate: up to 88.4% for 4.50 μm beads; efficiency increases with bead size | 281 |
| Lung adenocarcinoma cells | Immunomagnetic separation in serpentine microchannel | Capture rate >70% for A549 cells in less than 15 minutes; 4% capture of non-target cells | 282 |
| Cancerous cells | Dielectrophoresis-based microfluidic platform | Capture specificity up to 80.4% for A549 cells; LOD: 2 × 10$^4$ cells per mL | 283 |
| Lung carcinoma cells | Immunomagnetic separation in microfluidic channel | Capture efficiency: 77.8% | 284 |
| Circulating tumor cells | Tetrahedral DNA framework-based microfluidic technology; aptamer-hybridization chain reaction (Apt-HCR) | Capture efficiency: 83.3–94.2% for MCF-7 cells, release efficiency: 96.2% and 94.6% viability | 285 |
| CTCs | Fluidic multivalent membrane nanointerface; aptamer functionalized nanovesicles (Apt-nanovesicles); fluidic aptamer functionalized soft and high-affinity nanointerface microfluidic chip (FLASH-Chip) | Over 70% capture efficiency using artificial clinical samples, 7-fold higher capture efficiency than monovalent aptamer chip, 97.6% CTC viability after release | 286 |
| Different phenotypic CTCs (epithelial and mesenchymal) | Poly(lactic-co-glycolic acid) (PLGA) nanofiber microfluidic device with dual aptamers, captured by dual aptamers targeting EpCAM and N-cadherin | Capture efficiency: 91% for A2780 cells, 89% for OVCAR-3 cells; release efficiency: 95% (A2780), 88% (OVCAR-3) | 287 |
| CCRF-CEM cells (leukemia) | Thermo-chemo-mechanical coupling hydrogel in microfluidics; immunoaffinity-based cell catch – transport-release thermo-chemo-mechanical coupling hydrogel (iCatch) | Catching efficiency: ~40%, recovery rate: ~70%, high-throughput (~900 cells per mm s$^{-1}$) platform | 288 |
| Single circulating tumor cells (CTCs) - captured by dual multivalent aptamers | Dual-multivalent aptamer-conjugated nanoprobes; dual- multivalent-aptamers (DMAs), Sgc8 and SYL3C | Sorting separation rate: 93.6%; $K_d$: 0.26–0.34 nM; measurement efficiency: 73.8% | 289 |
| 3D tumor spheroids (MCF-7, A549) | Aptamer-modified gold nanoshells; photothermal therapy (PTT); NIR-absorbing hollow gold nanoshells; anti-MUC1 aptamer; HGN@anti-MUC1 | PTT efficiency increased by double irradiation; viability decreased by up to 69% (A549) | 148 |
| *Cryptosporidium parvum oocysts* | Microfluidic electrochemical biosensor with gold nano-/microislands (NMIs) | LOD: 5 oocysts per mL (buffer); LOD: 10 oocysts per mL (stool, tap water); detection range: 10–100 000 oocysts per mL | 290 |

**Table 9** *(continued)*

| Targets | Microfluidic methodology | Detection performance | Ref. |
|---------|--------------------------|----------------------|------|
| Bone microenvironment cells | Multicomponent bone-on-a-chip with TNF-α aptamer | Therapeutic potential of TNF-α aptamer in reducing TNF-α-induced cell damage in glucocorticoid-induced osteonecrosis model | 291 |

# 6. Microfluidics for aptamers in therapeutic applications

## 6.1 Aptamers and their applications in therapeutic applications

Several internationally recognized firms, including Aptamer Group, Base Pair Biotechnologies, Aptagen, SomaLogic, NeoVentures Biotechnology, Aptamer Sciences, TriLink BioTechnologies, and Vivonics, are engaged in the development of aptamers. Their efforts are directed towards agriculture, food safety, cancer diagnostics, drug development, and biosensing markets.[6] Notable examples of FDA-approved aptamers include Izervay (Astellas Pharma)[293] and Macugen (Pfizer),[294] both of which are utilized in the treatment of macular degeneration. Furthermore, significant advancements are being made in other aptamers as therapeutic agents.[16] For instance, AS1411 is currently in a phase-II clinical trial for treating metastatic renal cell carcinoma.[295] Aptamers have also been utilized in the identification of several endemic and epidemic diseases, such as cholera,[296] Crimean-Congo hemorrhagic fever,[297] meningitis,[298] sepsis,[299] tuberculosis,[300] Ebola,[301] influenza,[302] MERS-CoV,[303] SARS-CoV-2,[42] monkeypox,[304] smallpox,[305] and Zika/Dengue.[306]

## 6.2 Microfluidic technologies in aptamer development

Microfluidic technologies have revolutionized the screening of aptamers by providing miniaturized, integrated platforms for high-throughput, cost-effective, and precise screening processes. These systems simplify the aptamer selection process by combining synthesis, modification, and screening in a single device, greatly increasing screening efficiency. Rapid optimization of high-specificity and high-affinity aptamers is now promising for therapeutic applications such as targeted drug delivery and diagnostics, where precision and efficiency are critical. Integrated microfluidic systems (IMS) have accelerated aptamer development by automating processes that were previously carried out in resource-intensive settings. These platforms therefore provide precise control over reaction conditions, reduce sample and reagent consumption, and speed up discovery timelines. Their compact design allows for portability and usability in both clinical and laboratory settings. By taking these advantages, microfluidics provides a fast and efficient approach to aptamer development, meeting the growing demand for advanced therapeutic solutions.

## 6.3 Therapeutic aptamer screening and development

### 6.3.1 Recent innovations in aptamer drug-screening.
Aptamers have been demonstrated for drug-screening applications on microfluidic systems. For instance,

Balachandran et al.[307] developed a platform for the synthesis of aptamer-functionalized BioZIF-8 targeting lymph nodes and tumors on an IMC in a two-stage process, reducing synthesis time from 15 h to only 10 min and encapsulating more biomolecules compared to conventional methods. This platform also highlighted microfluidics' ability to reduce time and resources in aptamer development. Alternatively, Rouco et al.[308] demonstrated IMS effectiveness in surface modification of lipid-polymer hybrid nanoparticles, with microfluidics producing smaller particles (129 ± 1 nm) and a higher positive zeta potential (51 ± 1 mV). While microfluidics offered better control over particle synthesis and higher aptamer association efficiency (91 ± 2%), it was more complex and costly compared to traditional methods.[308] Moreover, Shan et al.[309] used a microfluidic mixing device (MMD) for small (diameter = 129 ± 5.5 nm) liposome formation at high encapsulation efficiency (90 ± 1.4%) for aptamers. Despite challenges in microchannel resolution and high fabrication costs, the MMD improved reproducibility and scalability, and even permitted successful *in vivo* tumor targeting and imaging.

## 6.4 Therapeutic applications of microfluidics-screened aptamers

### 6.4.1 Aptamers in personalized medicine.
Recent advancements in microfluidic systems have expanded the therapeutic applications of aptamers. For example, Xu et al.[310] integrated microfluidics into a liquid biopsy-guided drug release system for precision tumor therapy *via* aptamers. The study featured a magnetically controlled IMC that integrated CTC detection using aptamer-functionalized magnetic nanospheres with controlled drug release, adjusting doxorubicin delivery based on the number of captured tumor cells. This system provided high specificity for personalized cancer treatment, though its complexity, reliance on EpCAM expression, and potential microchannel fouling may limit clinical scalability. Yi et al.[311] highlighted that aptamer-functionalized exosomes combined with microfluidic chip, fluorescence-based detection, and SPR sensing for precise tumor targeting and drug delivery achieved high sensitivity in detecting tumor-derived exosomes (LOD ~ $10^5$ particles per mL). While this low-immunogenicity approach offers real-time, high-throughput analysis, challenges still remain in the time-consuming preparation of exosomes, lack of standardization, and expensive instrumentation required.

### 6.4.2 Microfluidic-aptamer synergies in targeted therapy.
The role of microfluidics in targeted therapy has been explored in thrombolysis studies for targeted therapy. For instance, one group[312] utilized a microfluidic model of

arterial occlusion to assess the thrombolytic efficacy of the RNA aptamer BB-031, which targeted von Willebrand Factor, to inhibit platelet aggregation, showing the most effective thrombolysis at 1692 nM BB-031.[312] The microfluidic system demonstrated a 17% reduction in thrombus surface area and 60% patency at this dose, but higher doses (3384 nM) were less effective, indicating potential off-target effects. Another group rapidly isolated anti-idiotype aptamers for SARS-CoV-2 spike protein quantification,[313] reducing the selection process to just five rounds in two days, and integrated these aptamers with graphene field-effect transistor (GFET) nanosensors for real-time, label-free detection in serum.[313] The aptamers exhibited strong binding affinities ($K_d$ from 32 ± 7 to 130 ± 25 nM) with detection limits as low as 1 pM, though the specialized equipment required for microfluidics and GFET may limit broader clinical accessibility.[313] It may be further used targeting SARS-CoV-2 viruses.

### 6.5 Clinical translation of aptamer-based therapeutics

Microfluidic systems have played a critical role in translating aptamer-based research to the clinic. For example, Nguyen *et al.*[314] developed a real-time monitoring platform for assessing drug responses in tumor biopsies, demonstrating the clinical relevance of aptamer-based therapies. This study employed a multi-well electrochemical aptasensor platform integrated with an IMC for label-free monitoring of apoptosis in micro-dissected tumor biopsies, detecting cytochrome C at a $K_d$ of 6.2 ± 1.6 ng mL$^{-1}$ across a dynamic range of 1 to 30 000 ng mL$^{-1}$. While the platform offered precise, high-throughput monitoring, its slow dissociation rate and complex fabrication might thwart widespread clinical use. Similarly, Zhu *et al.*[315] used aptamer-modified nanosubstrates to monitor lung cancer progression. Their polyethylene glycol-poly lactic acid-*co*-glycolic acid (PEG-PLGA) nanofiber microfluidic system, supplemented with a cocktail of aptamers, achieved >85% capture efficiency across four lung cancer cell lines and detected 3.5-fold more CTCs in mixed samples compared to traditional methods, which may be useful for theropetics.[315] While offering high sensitivity and specificity for real-time monitoring of clonal evolution, the platform's complexity in aptamer conjugation and the need for customized aptamers may limit its scalability. Nevertheless, these studies depict how microfluidics may facilitate the transition of aptamer research from preclinical stages to clinical therapies, significantly enhancing the precision and effectiveness of personalized medicine.

### 6.6 Advantages and challenges of microfluidics in aptamer-based therapeutics

While microfluidic systems have made significant advances in aptamer-based therapeutics, several challenges still remain. For instance, handling diverse biological samples such as primary cell cultures may introduces challenges, which may hinder reproducibility and consistency across

experiments. These issues are especially important in therapeutic applications, where high specificity and reproducibility are required for clinical use. Furthermore, the technical complexities of designing and operating IMS might present significant challenges. These systems frequently require specialized core knowledge and advanced equipment, making them inaccessible to research teams without extensive technical expertise. Moreover, the lack of standardization across microfluidic platforms also impedes scalability and clinical translation, complicating their integration into regulatory frameworks and real-world applications. Despite these challenges, ongoing advances in microfluidic design and automation show promise for overcoming these limitations. Improved system integration, reproducibility, and the development of standardized protocols will be critical to increasing the use of microfluidics in therapeutic settings. By overcoming these challenges, microfluidic systems can realize their full potential as transformative tools in the development of targeted aptamer-based treatments.

## 7. Challenges and perspectives

The traditional, on-bench SELEX process was once the cornerstone of aptamer selection having 1) been widely adopted over the past three decades and 2) paved the way for extensive exploration and application of these unique molecular probes. The major challenges of traditional SELEX can be summarized as follows. Firstly, binding of ssDNA libraries with target molecules is lengthy and inefficient. More importantly, the shear force during the binding process cannot be well controlled. Secondly, incomplete removal of unbound ssDNA and weakly-bound ssDNA due to residue issues in test tubes, which may be amplified by the subsequent round of PCR, reduces efficacy of screening process. Thirdly, the amplification of bound ssDNA requires off-chip PCR and human intervention, which cannot be automated. As a result, the total number of on-bench screening rounds may be at least 10–20, which may take weeks-months. More importantly, tedious post-SELEX processes are usually inevitable which can result in modified aptamer structures that then compromise their use in diverse applications. Furthermore, the number of screened candidates can be in the hundreds, which requires a large efforts and resources to identify the ones with optimal affinity and specificity.

Of these, the prolonged operational duration represents the most significant obstacle, and the one best-addressed by IMS over the past decade, as summarized below. Firstly, nano-beads with high surface-to-volume (S/V) ratios surface-coated with target molecules were used to enhance target-ssDNA binding within a short period of time (10–20 min for on-chip processes *vs.* weeks-months for on-bench processes), leading to a higher proportion of suitable aptamer candidate (dozens for on-chip processes *vs.* hundreds for traditional SELEX). Bead-based protocols which be easily performed on

microfluidic platforms may result in confirmed, limited candidates with higher performance in terms of affinity and specificity. Secondly, optimization of washing stringency, such as by controlling shearing forces generated by the micropumps (in the range of pN, which is close to the binding force between ssDNA & proteins) leads to more effective removal of non-specific or low-affinity candidates after binding processes. Thirdly, on-chip PCR integrated with the other functional microfluidic devices may eliminate off-chip processes and might reduce human intervention to where the entire screening process can be automated on a single chip. As a result, the lower samples and reagent volumes also lead to 10-fold or greater reductions in price.

To enhance the specificity of the screened aptamers, both negative selection using other proteins abundant in bio-samples and competitive selection using biosamples (such as blood or serum) were developed on microfluidic platforms. More importantly, by using AI-based bioinformatics (such as AlphaFold) to predict aptamer structures, binding sites, docking scores, hydrogen bond numbers, receptor–ligand numbers, free energies, interactive amino acid numbers, and nucleotide/total nucleotide ratios to target high-affinity/high-specificity aptamers from selected pools and binding of screened aptamers with target proteins, tedious post-SELEX processes can be significantly alleviated. As a result, modified aptamers with higher affinity and specificity may be available for clinical applications. Screened aptamers can be therefore used for rapid, sensitive diagnostics for cardiovascular diseases, cancer, diabetes, infectious diseases and many others by using novel, dual-aptamer assays to replace conventional immunoassays. It is envisioned that high-affinity, high-specificity aptamers may replace conventional antibodies, enabling sensitive detection and quantification of emerging biomarkers for a variety of biological applications.

## 8. Conclusions

In the past decade, significant advances in microfluidic SELEX have been demonstrated. Microfluidic platforms have transformed the SELEX process by combining synthesis, modification, and screening into a single compact system, allowing for precise control of reaction conditions while significantly reducing time, reagent consumption, and manual intervention. These advancements have enabled high-throughput, cost-effective, and precise aptamer screening, paving the way for a wide range of applications in diagnostics, therapeutics, and biosensing.

This review has introduced the impact of microfluidic technology on SELEX, emphasizing how integrated systems simplify and enhance various steps in the aptamer selection process. Advanced microfluidic methodologies were extensively reviewed for their use in screening aptamers for a variety of targets, including proteins, cells, and complex biological systems. Furthermore, the versatility of aptamers selected through microfluidic SELEX in applications such as personalized medicine and drug delivery was discussed.

Despite these advances, major challenges remain. These include the technical complexity of integrated microfluidic systems, variability in the handling of biological samples, and a lack of standardization across platforms, all of which restrict broader clinical adoption. Future efforts must focus on addressing these challenges by improving bioinformatics tools, standardizing microfluidic SELEX protocols, and creating scalable platforms for real-world use.

## Data availability

Data may be available provided by the corresponding author upon request.

## Author contributions

Yi-Da Chung: writing - original draft; Yi-Cheng Tsai; writing - original draft; Chi-Hung Wang: writing - original draft; Gwo-Bin Lee: writing - original draft, reviewing and editing.

## Conflicts of interest

There are no conflicts to declare.

## Acknowledgements

## References

1 M. Famulok, J. S. Hartig and G. Mayer, *Chem. Rev.*, 2007, **107**(9), 3715–3743.

2 K. M. Ahmad, S. S. Oh, S. Kim, F. M. McClellen, Y. Xiao and H. T. Soh, *PLoS One*, 2011, **6**(11), e27051.

3 M. Yüce, N. Ullah and H. Budak, *Analyst*, 2015, **140**, 5379–5399.

4 H. Kaur, J. G. Bruno, A. Kumar and T. K. Sharma, *Theranostics*, 2018, **8**(15), 4016–4032.

5 C. H. Weng, C. J. Huang and G. B. Lee, *Sensors*, 2012, **12**(7), 9514–9529.

6 K.-M. Song, S. Lee and C. Ban, *Sensors*, 2012, **12**(1), 612–631.

7 W. H. Thiel, T. Bair, A. S. Peek, X. Liu, J. Dassie, K. R. Stockdale, M. A. Behlke, F. J. Miller Jr and P. H. Giangrande, *PLoS One*, 2012, 7(9), e43836.

8 A. B. Iliuk, L. Hu and W. A. Tao, *Anal. Chem.*, 2011, **83**(12), 4440–4452.

9 D. Xiang, C. Zheng, S. F. Zhou, S. Qiao, P. H. L. Tran, C. Pu, Y. Li, L. Kong, A. Z. Kouzani, J. Lin, K. Liu, L. Li, S. Shigdar and W. Duan, *Theranostics*, 2015, **5**(10), 1083–1097.

10 L. Y. Wan, W. F. Yuan, W. B. Ai, Y. W. Ai, J. J. Wang, L. Y. Chu, Y. Q. Zhang and J. F. Wu, *Expert Opin. Drug Delivery*, 2019, **16**(3), 207–218.

11 S. Ni, Z. Zhuo, Y. Pan, Y. Yu, F. Li, J. Liu, L. Wang, X. Wu, D. Li, Y. Wan, L. Zhang, Z. Yang, B.-T. Zhang, A. Lu and G. Zhang, *ACS Appl. Mater. Interfaces*, 2021, **13**(8), 9500–9519.

12 H. Sun and Y. Zu, *Molecules*, 2015, **20**(7), 11959–11980.

13 N. K. Jain, H. C. Jetani and I. Roy, *Pharm. Res.*, 2013, **30**, 1871–1882.

14 J. Zhong, J. Ding, L. Deng, Y. Xiang, D. Liu, Y. Zhang, X. Chen and Q. Yang, *Drug Des., Dev. Ther.*, 2021, **15**, 3985–3996.

15 S. Liu, Y. Xu, X. Jiang, H. Tan and B. Ying, *Biosens. Bioelectron.*, 2022, **208**, 114168.

16 J. Zhou and J. Rossi, *Nat. Rev. Drug Discovery*, 2017, **16**, 181–202.

17 T. Wang, C. Chen, L. M. Larcher, R. A. Barrero and R. N. Veedu, *Biotechnol. Adv.*, 2019, **37**(1), 28–50.

18 H. Sun and Y. Zu, *Small*, 2015, **11**(20), 2352–2364.

19 A. Ruscito and M. C. DeRosa, *Front. Chem.*, 2016, **4**, 14.

20 Y. Zhang, B. S. Lai and M. Juhas, *Molecules*, 2019, **24**(5), 941.

21 M. Darmostuk, S. Rimpelova, H. Gbelcova and T. Ruml, *Biotechnol. Adv.*, 2015, **33**(6, Pt 2), 1141–1161.

22 Z. Zhuo, Y. Yu, M. Wang, J. Li, Z. Zhang, J. Liu, X. Wu, A. Lu, G. Zhang and B. Zhang, *Int. J. Mol. Sci.*, 2017, **18**(10), 2142.

23 S. I. Hori, A. Herrera, J. J. Rossi and J. Zhou, *Cancers*, 2018, **10**(1), 9.

24 H. Lin, W. Zhang, S. Jia, Z. Guan, C. J. Yang and Z. Zhu, *Biomicrofluidics*, 2014, **8**(4), 041501.

25 C. Tuerk and L. Gold, *Science*, 1990, **249**(4968), 505–510.

26 A. D. Ellington and J. W. Szostak, *Nature*, 1990, **346**, 818–822.

27 M. D. Leonida and I. Kumar, *Curr. Nanosci.*, 2012, **8**(3), 458–473.

28 G. T. Vladisavljević, N. Khalid, M. A. Neves, T. Kuroiwa, M. Nakajima, K. Uemura, S. Ichikawa and I. Kobayashi, *Adv. Drug Delivery Rev.*, 2013, **65**(11–12), 1626–1663.

29 D. G. Rackus, M. H. Shamsi and A. R. Wheeler, *Chem. Soc. Rev.*, 2015, **44**, 5320–5340.

30 A. G. Niculescu, C. Chircov, A. C. Bîrcă and A. M. Grumezescu, *Int. J. Mol. Sci.*, 2021, **22**(4), 2011.

31 T. M. Squires and S. R. Quake, *Rev. Mod. Phys.*, 2005, **77**, 977–1026.

32 P. N. Nge, C. I. Rogers and A. T. Woolley, *Chem. Rev.*, 2013, **113**(4), 2550–2583.

33 M. J. Jebrail, M. S. Bartsch and K. D. Patel, *Lab Chip*, 2012, **12**, 2452–2463.

34 J. B. Nielsen, R. L. Hanson, H. M. Almughamsi, C. Pang, T. R. Fish and A. T. Woolley, *Anal. Chem.*, 2020, **92**(1), 150–168.

35 R. Vitorino, S. Guedes, J. P. da Costa and V. Kašička, *Nanomaterials*, 2021, **11**(5), 1118.

36 C.-J. Huang, H.-I. Lin, S.-C. Shiesh and G.-B. Lee, *Biosens. Bioelectron.*, 2010, **25**(7), 1761–1766.

37 T. Olsen, J. Zhu, J. Kim, R. Pei, M. N. Stojanovic and Q. Lin, *SLAS Technol.*, 2017, **22**(1), 63–72.

38 D. N. Mazaafrianto, M. Maeki, A. Ishida, H. Tani and M. Tokeshi, *Micromachines*, 2018, **9**(5), 202.

39 W.-T. Liu, W.-B. Lee, Y.-C. Tsai, Y.-J. J. Chuang, K.-F. Hsu and G.-B. Lee, *Biomicrofluidics*, 2019, **13**(1), 014114.

40 C.-S. Lin, Y.-C. Tsai, K.-F. Hsu and G.-B. Lee, *Lab Chip*, 2021, **21**, 725–734.

41 R. Gandotra, H. B. Wu, P. Gopinathan, Y. C. Tsai, F. C. Kuo, M. S. Lee and G. B. Lee, *Lab Chip*, 2022, **22**, 250–261.

42 H.-B. Wu, C.-H. Wang, Y.-D. Chung, Y.-S. Shan, Y.-J. Lin, H.-P. Tsai and G.-B. Lee, *Anal. Chim. Acta*, 2023, **1274**, 341531.

43 R. Gandotra, H. B. Wu, F. C. Kuo, M. S. Lee and G. B. Lee, *ACS Sens.*, 2024, **9**(4), 1775–1784.

44 Y. Xu, X. Yang and E. Wang, *Anal. Chim. Acta*, 2010, **683**(1), 12–20.

45 S. K. Dembowski and M. T. Bowser, *Analyst*, 2018, **143**, 21–32.

46 S. D. Jayasena, *Clin. Chem.*, 1999, **45**(9), 1628–1650.

47 A. Ozer, J. M. Pagano and J. T. Lis, *Mol. Ther.–Nucleic Acids*, 2014, **3**, e183.

48 M. Blind and M. Blank, *Mol. Ther.–Nucleic Acids*, 2015, **4**, e223.

49 P. Bayat, R. Nosrati, M. Alibolandi, H. Rafatpanah, K. Abnous, M. Khedri and M. Ramezani, *Biochimie*, 2018, **154**, 132–155.

50 B. J. Hicke, C. Marion, Y. F. Chang, T. Gould, C. K. Lynott, D. Parma, P. G. Schmidt and S. Warren, *J. Biol. Chem.*, 2001, **276**(52), 48644–48654.

51 D. A. Daniels, H. Chen, B. J. Hicke, K. M. Swiderek and L. Gold, *Proc. Natl. Acad. Sci. U. S. A.*, 2003, **100**(26), 15416–15421.

52 D. Shangguan, Y. Li, Z. Tang, Z. C. Cao, H. W. Chen, P. Mallikaratchy, K. Sefah, C. J. Yang and W. Tan, *Proc. Natl. Acad. Sci. U. S. A.*, 2006, **103**(32), 11838–11843.

53 M. Ye, J. Hu, M. Peng, J. Liu, J. Liu, H. Liu, X. Zhao and W. Tan, *Int. J. Mol. Sci.*, 2012, **13**(3), 3341–3353.

54 L.-Y. Hung, C.-Y. Fu, C.-H. Wang, Y.-J. Chuang, Y.-C. Tsai, Y.-L. Lo, P.-H. Hsu, H.-Y. Chang, S.-C. Shiesh, K.-F. Hsu and G.-B. Lee, *Biomicrofluidics*, 2018, **12**(5), 054108.

55 S. D. Mendonsa and M. T. Bowser, *J. Am. Chem. Soc.*, 2004, **126**(1), 20–21.

56 M. Berezovski and S. N. Krylov, *J. Am. Chem. Soc.*, 2002, **124**(46), 13674–13675.

57 C. Zhu, G. Yang, M. Ghulam, L. Li and F. Qu, *Biotechnol. Adv.*, 2019, **37**(8), 107432.

58 R. Stoltenburg, N. Nikolaus and B. Strehlitz, *J. Anal. Methods Chem.*, 2012, **2012**, 415697.

59 N. Nikolaus and B. Strehlitz, *Sensors*, 2014, **14**(2), 3737–3755.

60 J. G. Bruno, *Biochem. Biophys. Res. Commun.*, 1997, **234**(1), 117–120.

61 X. Lou, J. Qian, Y. Xiao, L. Viel, A. E. Gerdon, E. T. Lagally, P. Atzberger, T. M. Tarasow, A. J. Heeger and H. T. Soh, *Proc. Natl. Acad. Sci. U. S. A.*, 2009, **106**(9), 2989–2994.

62 I. Manea, M. Casian, O. Hosu-Stancioiu, N. de-Los-Santos-Álvarez, M. J. Lobo-Castañón and C. Cristea, *Anal. Chim. Acta*, 2024, **1297**, 342325.

63 G. Hybarger, J. Bynum, R. F. Williams, J. J. Valdes and J. P. Chambers, *Anal. Bioanal. Chem.*, 2006, **384**, 191–198.

64  R. K. Mosing and M. T. Bowser, *J. Sep. Sci.*, 2007, **30**(10), 1420–1426.

65  G. Aquino-Jarquin and J. D. Toscano-Garibay, *Int. J. Mol. Sci.*, 2011, **12**(12), 9155–9171.

66  C. Zhu, Z. Feng, H. Qin, L. Chen, M. Yan, L. Li and F. Qu, *Talanta*, 2024, **266**(Pt 1), 124998.

67  Z. Fang, X. Feng, F. Tang, H. Jiang, S. Han, R. Tao and C. Lu, *Biosensors*, 2024, **14**(7), 350.

68  N. K. Singh, Y. Wang, C. Wen, B. Davis, X. Wang, K. Lee and Y. Wang, *Nat. Biotechnol.*, 2023, **42**, 1224–1231.

69  L. Y. Hung, C. H. Wang, C. Y. Fu, P. Gopinathan and G. B. Lee, *Lab Chip*, 2016, **16**, 2759–2774.

70  L. A. Fraser, Y.-W. Cheung, A. B. Kinghorn, W. Guo, S. C.-C. Shiu, C. Jinata, M. Liu, S. Bhuyan, L. Nan, H. C. Shum and J. A. Tanner, *Adv. Biosyst.*, 2019, **3**(5), 1900012.

71  Y. Liu, N. Wang, C.-W. Chan, A. Lu, Y. Yu, G. Zhang and K. Ren, *Front. Cell Dev. Biol.*, 2021, **9**, 730035.

72  L. Gold, B. Polisky, O. Uhlenbeck and M. Yarus, *Annu. Rev. Biochem.*, 1995, **64**, 763–797.

73  Y. Yu, C. Liang, Q. Lv, D. Li, X. Xu, B. Liu, A. Lu and G. Zhang, *Int. J. Mol. Sci.*, 2016, **17**(3), 358.

74  J. C. Chaput, *Acc. Chem. Res.*, 2021, **54**(4), 1056–1065.

75  A. C. Larsen, M. R. Dunn, A. Hatch, S. P. Sau, C. Youngbull and J. C. Chaput, *Nat. Commun.*, 2016, **7**, 11235.

76  D. Vallejo, A. Nikoomanzar, B. M. Paegel and J. C. Chaput, *ACS Synth. Biol.*, 2019, **8**(6), 1430–1440.

77  A. Nikoomanzar, D. Vallejo, E. J. Yik and J. C. Chaput, *ACS Synth. Biol.*, 2020, **9**(7), 1873–1881.

78  M. Cho, S. S. Oh, J. Nie, R. Stewart, M. J. Radeke, M. Eisenstein, P. J. Coffey, J. A. Thomson and H. T. Soh, *Anal. Chem.*, 2015, **87**(1), 821–828.

79  Y. Sheng and M. T. Bowser, *Analyst*, 2013, **139**, 215–224.

80  S. H. Lee, J. H. Lee, H. W. Lee, Y.-H. Kim, O. C. Jeong and J.-Y. Ahn, *PLoS One*, 2016, **11**, e0159777.

81  S. H. Lee, H. W. Lee, D. S. Kim, H. G. Kwon, J. H. Lee, Y.-H. Kim, O. C. Jeong and J.-Y. Ahn, *J. Visualized Exp.*, 2018, **141**, e57703.

82  D. Chang, Z. Wang, C. D. Flynn, A. Mahmud, M. Labib, H. Wang, A. Geraili, X. Li, J. Zhang, E. H. Sargent and S. O. Kelley, *Nat. Chem.*, 2023, **15**, 773–780.

83  C. M. Birch, H. W. Hou, J. Han and J. C. Niles, *Sci. Rep.*, 2015, **5**, 11347.

84  J. P. Hilton, T. Olsen, J. Kim, J. Zhu, T. H. Nguyen, M. Barbu, R. Pei, M. Stojanovic and Q. Lin, *Microfluid. Nanofluid.*, 2015, **19**, 795–804.

85  T. R. Olsen, C. Tapia-Alveal, K.-A. Yang, X. Zhang, L. J. Pereira, N. Farmakidis, R. Pei, M. N. Stojanovic and Q. Lin, *J. Electrochem. Soc.*, 2017, **164**(5), B3122–B3129.

86  T. R. Olsen, C. Tapia-Alveal, K. Wen, T. S. Worgall, M. N. Stojanovic and Q. Lin, *Biomed. Microdevices*, 2023, **25**, 3.

87  J. Kim, T. R. Olsen, J. Zhu, J. P. Hilton, K.-A. Yang, R. Pei, M. N. Stojanovic and Q. Lin, *Sci. Rep.*, 2016, **6**, 26139.

88  K. Wen, Y. Chen, X. Meng, S. Botros, W. Dai, M. N. Stojanovic, R. Tomer and Q. Lin, *Microchem. J.*, 2023, **188**, 108454.

89  X. Meng, K. Wen, M. Citartan and Q. Lin, *Analyst*, 2022, **148**, 787–798.

90  S. Chung, N. G. Gurudatt, J. Jeon, C. Ban and Y.-B. Shim, *Anal. Chem.*, 2021, **93**(3), 1416–1422.

91  Y. Lu, S. Yu, F. Lin, F. Lin, X. Zhao, L. Wu, Y. Miao, H. Li, Y. Deng and L. Geng, *Analyst*, 2017, **142**, 4257–4264.

92  J.-W. Park, S. J. Lee, S. Ren, S. Lee, S. Kim and T. Laurell, *Sci. Rep.*, 2016, **6**, 27121.

93  C. Bai, X. Meng, K. Wen, M. Citartan, C. Wang, S. Yu and Q. Lin, *Microfluid. Nanofluid.*, 2022, **26**, 43.

94  K. Z. Yang, M. Wang, M. Y. Gao, Y. T. Wang and Z. L. Zhang, *Chem. Commun.*, 2024, **60**, 2772–2775.

95  H. Lim, J. Chang, K.-I. Kim, Y. Moon, S. Lee, B. Lee, J. H. Lee and J. Lee, *Biomicrofluidics*, 2022, **16**(4), 044102.

96  D. Chen, Y. Orenstein, R. Golodnitsky, M. Pellach, D. Avrahami, C. Wachtel, A. Ovadia-Shochat, H. Shir-Shapira, A. Kedmi, T. Juven-Gershon, R. Shamir and D. Gerber, *Sci. Rep.*, 2016, **6**, 33351.

97  X. Liu, H. Li, W. Jia, Z. Chen and D. Xu, *Lab Chip*, 2017, **17**, 178–185.

98  H.-I. Lin, C.-C. Wu, C.-H. Yang, K.-W. Chang, G.-B. Lee and S.-C. Shiesh, *Lab Chip*, 2015, **15**, 486–494.

99  J. Soundy and D. Day, *PLoS One*, 2017, **12**(9), e0185385.

100  H. Stoll, H. Kiessling, M. Stelzle, H. P. Wendel, J. Schütte, B. Hagmeyer and M. Avci-Adali, *Biomicrofluidics*, 2015, **9**(3), 034111.

101  L.-Y. Hung, C.-H. Wang, K.-F. Hsu, C.-Y. Chou and G.-B. Lee, *Lab Chip*, 2014, **14**, 4017–4028.

102  L. Y. Hung, C. H. Wang, Y. J. Che, C. Y. Fu, H. Y. Chang, K. Wang and G. B. Lee, *Sci. Rep.*, 2015, **5**, 10326.

103  P. Gopinathan, L.-Y. Hung, C.-H. Wang, N.-J. Chiang, Y.-C. Wang, Y.-S. Shan and G.-B. Lee, *Biomicrofluidics*, 2017, **11**, 044101.

104  J. Chen, X. Liu, M. Xu, Z. Li and D. Xu, *Biomicrofluidics*, 2021, **15**(2), 024107.

105  E. Dausse, A. Barré, A. Aimé, A. Groppi, A. Rico, C. Ainali, G. Salgado, W. Palau, E. Daguerre, M. Nikolski, J.-J. Toulmé and C. Di Primo, *Biosens. Bioelectron.*, 2016, **80**, 418–425.

106  I. Anosova, E. A. Kowal, M. R. Dunn, J. C. Chaput, W. D. V. Horn and M. Egli, *Nucleic Acids Res.*, 2016, **44**, 1007–1021.

107  S. Ohuchi, *BioRes. Open Access*, 2012, **1**(6), 265–272.

108  S. Catuogno and C. L. Esposito, *Biomedicines*, 2017, **5**(3), 49.

109  J. Dai, J. Li, Y. Jiao, X. Yang, D. Yang, Z. Zhong, H. Li and Y. Yang, *Food Chem.*, 2024, **456**, 139955.

110  Z. Khoshbin, M. Moeenfard, K. Abnous and S. M. Taghdisi, *Food Chem.*, 2023, **399**, 133983.

111  C.-H. Wang and G.-B. Lee, *Biomicrofluidics*, 2020, **14**(2), 024110.

112  Y. Lu, J. Wen, C. Wang, M. Wang, F. Jiang, L. Miao, M. Xu, Y. Li, X. Chen and Y. Chen, *Small*, 2024, **20**(20), 2308424.

113  C. J. Huang, H. I. Lin, S. C. Shiesh and G. B. Lee, *Biosens. Bioelectron.*, 2012, **35**(1), 50–55.

114  A. Sinha, P. Gopinathan, Y. D. Chung, H. Y. Lin, K. H. Li, H. P. Ma, P. C. Huang, S. C. Shiesh and G. B. Lee, *Biosens. Bioelectron.*, 2018, **122**, 104–112.

115  S. Shin, B. Kim, Y.-J. J. Kim and S. Choi, *Biosens. Bioelectron.*, 2019, **133**, 169–176.

116  K. R. Wehmeyer, R. J. White, P. T. Kissinger and W. R. Heineman, *Annu. Rev. Anal. Chem.*, 2021, **14**, 109–131.

117  S. Saito, *Anal. Sci.*, 2021, **37**, 17–26.

118  S.-C. Tsai, L.-Y. Hung and G.-B. Lee, *Biomicrofluidics*, 2017, **11**(3), 034122.

119  Q. Wang, W. Liu, Y. Xing, X. Yang, K. Wang, R. Jiang, P. Wang and Q. Zhao, *Anal. Chem.*, 2014, **86**(13), 6572–6579.

120  R. Su, Z. Li, C. Yang, Y. Li, J. Wang and C. Sun, *Spectrochim. Acta, Part A*, 2024, **320**, 124643.

121  Z. Di, J. Zhao, H. Chu, W. Xue, Y. Zhao and L. Li, *Adv. Mater.*, 2019, **31**(33), 1901885.

122  A. Marton Menendez and D. J. Nesbitt, *J. Phys. Chem. B*, 2022, **126**(1), 69–79.

123  A. Espah Borujeni, D. M. Mishler, J. Wang, W. Huso and H. M. Salis, *Nucleic Acids Res.*, 2016, **44**(1), 1–13.

124  L. Bao and Y. Xiao, Exploring the Binding Process of Cognate Ligand to *Add* Adenine Riboswitch Aptamer by Using Explicit Solvent Molecular Dynamics (MD) Simulation, in *RNA Structure and Dynamics*, ed. Y.-X. Wang, J. R. Stagno and J. Ding, Methods in Molecular Biology, Humana, New York, 1st edn, 2023, pp. 103–122.

125  L. M. Hertz, E. N. White, K. Kuznedelov, L. Cheng, A. M. Yu, R. Kakkaramadam, K. Severinov, A. Chen and J. B. Lucks, *Nucleic Acids Res.*, 2024, **52**(8), 4466–4482.

126  Y. Tian, S. Zhang, L. Wang and S. Liu, *ChemBioChem*, 2018, **19**(7), 716–722.

127  V. Esposito, A. Russo, V. Vellecco, M. Bucci, G. Russo, L. Mayol, A. Virgilio and A. Galeone, *Biochim. Biophys. Acta, Gen. Subj.*, 2018, **1862**(12), 2645–2650.

128  Y. Takeuchi, M. Endo, Y. Suzuki, K. Hidaka, G. Durand, E. Dausse, J.-J. Toulmé and H. Sugiyama, *Biomater. Sci.*, 2016, **4**, 130–135.

129  A. Gupta and M. Bansal, *Phys. Chem. Chem. Phys.*, 2016, **18**, 28767–28780.

130  L. V. Croft, M. Fisher, T. K. Barbhuiya, S. El-Kamand, S. Beard, A. Rajapakse, R. Gamsjaeger, L. Cubeddu, E. Bolderson, K. O'Byrne, D. Richard and N. S. Gandhi, *Nucleic Acid Ther.*, 2024, **34**(3), 143–155.

131  R. Pal, I. Deb, J. Sarzynska and A. Lahiri, *J. Biomol. Struct. Dyn.*, 2023, **41**(6), 2221–2230.

132  H. Komine, S. Mori, K. Morihiro, K. Ishida, T. Okuda, Y. Kasahara, H. Aoyama, T. Yamaguchi and S. Obika, *Molecules*, 2020, **25**(7), 1732.

133  B. Niu, Y. Wu, M. Zhou, R. Lin, P. Ge, X. Chen, H. Zhou, X. Zhang and J. Xie, *Cancer Lett.*, 2023, **579**, 216461.

134  Y. Kazemi, S. Dehghani, F. Soltani, K. Abnous, M. Alibolandi, S. M. Taghdisi and M. Ramezani, *Nanomedicine*, 2022, **45**, 102588.

135  J. Rihon, C.-A. Mattelaer, R. W. Montalvão, M. Froeyen, V. B. Pinheiro and E. Lescrinier, *Nucleic Acids Res.*, 2024, **52**(6), 2836–2847.

136  C. Riccardi, E. Napolitano, D. Musumeci and D. Montesarchio, *Molecules*, 2020, **25**(22), 5227.

137  L. Yao, L. Wang, S. Liu, H. Qu, Y. Mao, Y. Li and L. Zheng, *Chem. Sci.*, 2024, **15**, 13011–13020.

138  C.-H. Wang, C.-P. Chang and G.-B. Lee, *Biosens. Bioelectron.*, 2016, **86**, 247–254.

139  I. de F. Souza, J. P. de J. Vieira, E. D. Bonifácio, B. A. de Avelar Freitas and L. A. G. Torres, *Tissue Eng., Part B*, 2024, DOI: **10.1089/ten.teb.2024.0088**.

140  C. Tian, S. Zheng, X. Liu and K.-I. Kamei, *J. Nanobiotechnol.*, 2022, **20**, 338.

141  J.-L. Chang, C.-J. Huang, Y.-C. Tsai, N.-J. Chiang, Y.-S. Huang, S.-C. Hung, Y.-S. Shan and G.-B. Lee, *Lab Chip*, 2024, **24**, 375–382.

142  P. Gopinathan, N. J. Chiang, A. Bandaru, A. Sinha, W. Y. Huang, S. C. Hung, Y. S. Shan and G. B. Lee, *Adv. Healthcare Mater.*, 2020, **9**(10), 1901875.

143  C. Wang, J. Qiu, M. Liu, Y. Wang, Y. Yu, H. Liu, Y. Zhang and L. Han, *Adv. Sci.*, 2024, **11**(28), 240163.

144  W.-J. Soong, C.-H. Wang, C. Chen and G.-B. Lee, *Lab Chip*, 2024, **24**, 1965–1976.

145  V. Bonnet, E. Maikranz, M. Madec, N. Vertti-Quintero, C. Cuche, M. Mastrogiovanni, A. Alcover, V. Di Bartolo and C. N. Baroud, *Proc. Natl. Acad. Sci. U. S. A.*, 2024, **121**(11), e2316500121.

146  P. Xu, J. Chi, X. Wang, M. Zhu, K. Chen, Q. Fan, F. Ye and C. Shao, *Lab Chip*, 2024, **24**, 3470–3479.

147  D. Sun, Y. Ma, M. Wu, Z. Chen, L. Zhang and J. Lu, *J. Pharm. Anal.*, 2023, **13**(4), 340–354.

148  D. Kalinowska, I. Grabowska-Jadach, M. Liwinska, M. Drozd, M. Pietrzak, A. Dybko and Z. Brzozka, *Biosens. Bioelectron.*, 2019, **126**, 214–221.

149  A. M. Rodríguez-Ces, Ó. Rapado-González, Á. Salgado-Barreira, M. A. Santos, C. Aroso, A. S. Vinhas, R. López-López and M. M. Suárez-Cunqueiro, *Diagnostics*, 2024, **14**(14), 1465.

150  C.-H. Wang, Y.-S. Shao, K.-F. Hsu and G.-B. Lee, *Chem. Eng. J.*, 2024, **495**, 153478.

151  M. Kohlberger and G. Gadermaier, *Biotechnol. Appl. Biochem.*, 2022, **69**(5), 1771–1792.

152  M. Berezovski, M. Musheev, A. Drabovich and S. N. Krylov, *J. Am. Chem. Soc.*, 2006, **128**(5), 1410–1411.

153  J. Tok, J. Lai, T. Leung and S. F. Y. Li, *Electrophoresis*, 2010, **31**(12), 2055–2062.

154  M. V. Berezovski, M. U. Musheev, A. P. Drabovich, J. V. Jitkova and S. N. Krylov, *Nat. Protoc.*, 2006, **1**, 1359–1369.

155  W. Pan, P. Xin and G. A. Clawson, *BioTechniques*, 2008, **44**, 351–360.

156  W. Pan and G. A. Clawson, *Molecules*, 2009, **14**(4), 1353–1369.

157  Z. Xi, R. Huang, Y. Deng and N. He, *J. Biomed. Nanotechnol.*, 2014, **10**(10), 3043–3062.

158  S. D. Mendonsa and M. T. Bowser, *Anal. Chem.*, 2004, **76**(18), 5387–5392.

159  R. K. Mosing, S. D. Mendonsa and M. T. Bowser, *Anal. Chem.*, 2005, **77**(19), 6107–6112.

160  G. T. Rozenblum, V. G. Lopez, A. D. Vitullo and M. Radrizzani, *Expert Opin. Drug Discovery*, 2016, **11**(2), 127–135.

161 W. He, M. A. Elizondo-Riojas, X. Li, G. L. R. Lokesh, A. Somasunderam, V. Thiviyanathan, D. E. Volk, R. H. Durland, J. Englehardt, C. N. Cavasotto and D. G. Gorenstein, *Biochemistry*, 2012, **51**(42), 8321–8323.

162 S. Lisi, E. Fiore, S. Scarano, E. Pascale, Y. Boehman, F. Ducongé, S. Chierici, M. Minunni, E. Peyrin and C. Ravelet, *Anal. Chim. Acta*, 2018, **1038**, 173–181.

163 G. Yang, C. Zhu, L. Zhao, L. Li, Y. Huang, Y. Zhang and F. Qu, *Chin. Chem. Lett.*, 2021, **32**(1), 218–220.

164 H. R. Kim, M. Y. Song and B. C. Kim, *Anal. Biochem.*, 2020, **591**, 113542.

165 M. Liu, L. Geng, F. Zhang, S. Dou, F. Li, Z. Liu, Y. Guo and X. Sun, *J. Agric. Food Chem.*, 2022, **70**(50), 15990–15998.

166 I. H. Jeong, H. K. Kim, H. R. Kim, J. Kim and B. C. Kim, *Anal. Bioanal. Chem.*, 2022, **414**, 7763–7771.

167 M. J. N. Tapp, J. M. Slocik, P. B. Dennis, R. R. Naik and V. T. Milam, *ACS Comb. Sci.*, 2018, **20**(10), 585–593.

168 R. Sullivan, M. C. Adams, R. R. Naik and V. T. Milam, *Molecules*, 2019, **24**(8), 1572.

169 A. Kushwaha, Y. Takamura, K. Nishigaki and M. Biyani, *Sci. Rep.*, 2019, **9**, 6642.

170 D. Wu, T. Feagin, P. Mage, A. Rangel, L. Wan, D. Kong, A. Li, J. Coller, M. Eisenstein and H. Soh, *Anal. Chem.*, 2023, **95**(5), 2645–2652.

171 M. Biyani, K. Yasuda, Y. Isogai, Y. Okamoto, W. Weilin, N. Kodera, H. Flechsig, T. Sakaki, M. Nakajima and M. Biyani, *ACS Appl. Mater. Interfaces*, 2022, **14**(16), 18064–18078.

172 A. Parashar, V. Bhushan, N. C. Mahanandia, S. Kumar and A. K. Mohanty, *J. Dairy Sci.*, 2022, **105**(7), 5545–5560.

173 A. Lozoya-Colinas, Y. Yu and J. C. Chaput, *J. Am. Chem. Soc.*, 2023, **145**(47), 25789–25796.

174 A. M. Yoshikawa, A. E. Rangel, L. Zheng, L. Wan, L. A. Hein, A. A. Hariri, M. Eisenstein and H. T. Soh, *Nat. Commun.*, 2023, **14**, 2336.

175 H. Sun, W. Tan and Y. Zu, *Analyst*, 2016, **141**, 403–415.

176 V. Thiviyanathan and D. G. Gorenstein, *Proteomics: Clin. Appl.*, 2012, **6**(11–12), 563–573.

177 E. Torres-Chavolla and E. C. Alocilja, *Biosens. Bioelectron.*, 2009, **24**(11), 3175–3182.

178 O. Alkhamis, J. Canoura, H. Yu, Y. Liu and Y. Xiao, *TrAC, Trends Anal. Chem.*, 2019, **121**, 115699.

179 A. D. Gelinas, D. R. Davies and N. Janjic, *Curr. Opin. Struct. Biol.*, 2016, **36**, 122–132.

180 T. Hermann and D. J. Patel, *Science*, 2000, **287**(5454), 820–825.

181 Y. Nomura, S. Sugiyama, T. Sakamoto, S. Miyakawa, H. Adachi, K. Takano, S. Murakami, T. Inoue, Y. Mori, Y. Nakamura and H. Matsumura, *Nucleic Acids Res.*, 2010, **38**(21), 7822–7829.

182 X. Hao, P. Yeh, Y. Qin, Y. Jiang, Z. Qiu, S. Li, T. Le and X. Cao, *Anal. Chim. Acta*, 2019, **1056**, 96–107.

183 V. Parkula, M. Berto, C. Diacci, B. Patrahau, M. Di Lauro, A. Kovtun, A. Liscio, M. Sensi, P. Samorì, P. Greco, C. A. Bortolotti and F. Biscarini, *Anal. Chem.*, 2020, **92**(13), 9330–9337.

184 X. Wang, X. He, Z. He, L. Hou, C. Ge, L. Wang, S. Li and Y. Xu, *Biosens. Bioelectron.*, 2022, **204**, 114057.

185 F. Pfeiffer and G. Mayer, *Front. Chem.*, 2016, **4**, 25.

186 Z. Li, M. A. Mohamed, A. M. Vinu Mohan, Z. Zhu, V. Sharma, G. K. Mishra and R. K. Mishra, *Sensors*, 2019, **19**(24), 5435.

187 G. K. Mishra, V. Sharma and R. K. Mishra, *Biosensors*, 2018, **8**(2), 28.

188 X. Chen, J. Wang, H. Y. Shen, X. Su, Y. Cao, T. Li and N. Gan, *ACS Sens.*, 2019, **4**(8), 2131–2139.

189 M. Park and T. S. Seo, *Biosens. Bioelectron.*, 2019, **126**, 405–411.

190 W.-H. Huang, V.-P. Mai, R.-Y. Wu, K.-L. Yeh and R.-J. Yang, *Micromachines*, 2011, **12**(11), 1283.

191 S. Qian, Y. Han, F. Xu, D. Feng, X. Yang, X. Wu, L. Hao and M. Yuan, *Talanta*, 2022, **247**, 123548.

192 K. Yoshida, T. Hayashi, M. Takinoue and H. Onoe, *Sci. Rep.*, 2022, **12**, 9692.

193 A. M. Ulloa-Gomez, A. Lucas, A. Koneru, A. Barui and L. Stanciu, *Biosens. Bioelectron.*, 2023, **221**, 114419.

194 C. C. Tseng, S. Y. Lu, S. J. Chen, J. M. Wang, L. M. Fu and Y. H. Wu, *Anal. Chim. Acta*, 2022, **1203**, 339722.

195 F. Chen, J. Wang, L. Du, X. Zhang, F. Zhang, W. Chen, W. Cai, C. Wu and P. Wang, *Biosens. Bioelectron.*, 2019, **130**, 382–388.

196 B. Chen, D. Wang, S. Wei and J. Wang, *Biosens. Bioelectron.*, 2024, **260**, 116434.

197 Z. Ji, D. Wang and J. Wang, *Anal. Methods*, 2024, **16**, 4160–4167.

198 A. M. Ulloa-Gomez, J. F. Waimin, Y. C. Yu, A. Lucas and L. A. Stanciu, *Microchim. Acta*, 2024, **191**, 194.

199 X. Chen, Y. Liu, X. Fang, Z. Li, H. Pu, J. Chang, J. Chen and S. Mao, *Biosens. Bioelectron.*, 2019, **126**, 664–671.

200 F. Costantini, N. Lovecchio, A. Ruggi, C. Manetti, A. Nascetti, M. Reverberi, G. de Cesare and D. Caputo, *ACS Appl. Bio Mater.*, 2019, **2**(12), 5880–5887.

201 L. He, Z. Shen, Y. Cao, T. Li, D. Wu, Y. Dong and N. Gan, *Analyst*, 2019, **144**, 2755–2764.

202 N. Nekrasov, D. Kireev, A. Emelianov and I. Bobrinetskiy, *Toxins*, 2019, **11**(10), 550.

203 S. Ramalingam, R. Chand, C. B. Singh and A. Singh, *Biosens. Bioelectron.*, 2019, **135**, 14–21.

204 L. He, Z. Shen, J. Wang, J. Zeng, W. Wang, H. Wu, Q. Wang and N. Gan, *Microchim. Acta*, 2020, **187**, 176.

205 A. Kasoju, D. Shahdeo, A. A. Khan, N. S. Shrikrishna, S. Mahari, A. M. Alanazi, M. A. Bhat, J. Giri and S. Gandhi, *Sci. Rep.*, 2020, **10**, 4627.

206 R. Tian, J. Ji, Y. Zhou, Y. Du, X. Bian, F. Zhu, G. Liu, S. Deng, Y. Wan and J. Yan, *Biosens. Bioelectron.*, 2020, **160**, 112218.

207 Z. Khoshbin, K. Abnous, S. M. Taghdisi and A. Verdian, *Biosens. Bioelectron.*, 2021, **191**, 113457.

208 S. Ramalingam, A. Elsayed and A. Singh, *Food Chem.*, 2023, **403**, 134302.

209 L. Kékedy-Nagy, J. M. Perry, S. R. Little, O. Y. Llorens and S. C. C. Shih, *Biosens. Bioelectron.*, 2023, **222**, 114998.

210 P. Wang, L. Ding, Y. Zhang and X. Jiang, *Biosensors*, 2023, **13**(12), 1027.

211 X. Zhou, Z. Sun, X. Su, K. Zheng, X. Zou and W. Zhang, *Anal. Chem.*, 2023, **95**(3), 1916–1923.

212 W. Ma, L. Liu, Y. Xu, L. Wang, L. Chen, S. Yan, L. Shui, Z. Wang and S. Li, *Analyst*, 2020, **145**, 4204–4211.

213 A. Nascetti, M. Mirasoli, E. Marchegiani, M. Zangheri, F. Costantini, A. Porchetta, L. Iannascoli, N. Lovecchio, D. Caputo, G. de Cesare, S. Pirrotta and A. Roda, *Biosens. Bioelectron.*, 2019, **123**, 195–203.

214 J. Niu, X. Hu, W. Ouyang, Y. Chen, S. Liu, J. Han and L. Liu, *Anal. Chem.*, 2019, **91**(3), 2360–2367.

215 M. Nandimandalam, F. Costantini, N. Lovecchio, L. Iannascoli, A. Nascetti, G. de Cesare, D. Caputo and C. Manetti, *Materials*, 2021, **14**(23), 7210.

216 X. Weng, Z. Fu, C. Zhang, W. Jiang and H. Jiang, *Anal. Chem.*, 2022, **94**(8), 3526–3534.

217 M. Afzal, J. Park, J. S. Jeon, M. Akmal, T.-S. Yoon and H. J. Sung, *Anal. Chem.*, 2021, **93**(23), 8309–8317.

218 N. Ardoino, L. Lunelli, G. Pucker, L. Vanzetti, R. Favaretto, L. Pasquardini, C. Pederzolli, C. Guardiani and C. Potrich, *Sensors*, 2024, **24**(10), 3107.

219 S. Arshavsky-Graham, A. Enders, S. Ackerman, J. Bahnemann and E. Segal, *Microchim. Acta*, 2021, **188**, 67.

220 F. R. Cavallo, K. B. Mirza, S. de Mateo, K. Nikolic, J. Rodriguez-Manzano and C. Toumazou, *ACS Sens.*, 2021, **6**(3), 709–715.

221 R. Gandotra, F. C. Kuo, M. S. Lee and G. B. Lee, *Anal. Chim. Acta*, 2023, **1281**, 341879.

222 C. Ge, J. Feng, J. Zhang, K. Hu, D. Wang, L. Zha, X. Hu and R. Li, *Talanta*, 2022, **236**, 122847.

223 H. Jiang, Q. Guo, C. Zhang, Z. Sun and X. Weng, *Food Chem.*, 2021, **365**, 130511.

224 N. I. Khan, M. Mousazadehkasin, S. Ghosh, J. G. Tsavalas and E. Song, *Analyst*, 2020, **145**, 4494–4503.

225 S. H. Lee, B. Cha, J. Ko, M. Afzal and J. Park, *Biomicrofluidics*, 2023, **17**, 024105.

226 P. R. Li, S. K. Boilla, C. H. Wang, P. C. Lin, C. N. Kuo, T. H. Tsai and G. B. Lee, *Biosens. Bioelectron.*, 2024, **249**, 115931.

227 R. S. Massey, E. M. McConnell, D. Chan, M. R. Holahan, M. C. DeRosa and R. Prakash, *ACS Sens.*, 2023, **8**(8), 3116–3126.

228 T. T. Q. Nguyen, E. M. Lee, T. T. T. Dang, E. R. Kim, Y. Ko and M. B. Gu, *Biosens. Bioelectron.*, 2024, **251**, 116097.

229 A. M. Ogunmolasuyi, R. Fogel, H. Hoppe, D. Goldring and J. Limson, *Malar. J.*, 2022, **21**, 174.

230 M. Pan, X. Han, S. Chen, J. Yang, Y. Wang, H. Li and S. Wang, *Talanta*, 2024, **267**, 125188.

231 S. Ramalingam, A. Elsayed and A. Singh, *Microchim. Acta*, 2020, **187**(12), 645.

232 Y. Su, W. Lai, Y. Liang and C. Zhang, *Anal. Chim. Acta*, 2022, **1206**, 339789.

233 A. M. Ulloa-Gomez, A. Agredo, A. Lucas, S. B. Somvanshi and L. Stanciu, *Biosens. Bioelectron.*, 2023, **222**, 114938.

234 J. Xue, L. Zhang, C. Gao, P. Zhu and J. Yu, *Biosens. Bioelectron.*, 2019, **133**, 1–7.

235 X. Zhang, X. Wei, C. X. Wu, X. Men, J. Wang, J. J. Bai, X. Y. Sun, Y. Wang, T. Yang, C. T. Lim, M. L. Chen and J. H. Wang, *ACS Nano*, 2024, **18**(8), 6612–6622.

236 A. Sinha, T. Y. Tai, K. H. Li, P. Gopinathan, Y. D. Chung, I. Sarangadharan, H. P. Ma, P. C. Huang, S. C. Shiesh, Y. L. Wang and G. B. Lee, *Biosens. Bioelectron.*, 2019, **129**, 155–163.

237 S. S. T. Gamage, T. N. Pahattuge, H. Wijerathne, K. Childers, S. Vaidyanathan, U. S. Athapattu, L. Zhang, Z. Zhao, M. L. Hupert, R. M. Muller, J. Muller-Cohn, J. Dickerson, D. Dufek, B. V. Geisbrecht, H. Pathak, Z. Pessetto, G. N. Gan, J. Choi, S. Park, A. K. Godwin, M. A. Witek and S. A. Soper, *Sci. Adv.*, 2022, **8**(39), eabn9665.

238 Y. Huang, Q. Wu, J. Zhang, Y. Zhang, S. Cen, C. Yang and Y. Song, *ACS Nano*, 2023, **17**(21), 21973–21983.

239 N. Saraf, M. Villegas, B. J. Willenberg and S. Seal, *ACS Omega*, 2019, **4**(1), 2234–2240.

240 L. Xu, S. Ramadan, B. G. Rosa, Y. Zhang, T. Yin, E. Torres, O. Shaforost, A. Panagiotopoulos, B. Li, G. Kerherve, D. K. Kim, C. Mattevi, L. R. Jiao, P. K. Petrov and N. Klein, *Sens. Diagn.*, 2022, **1**, 719–730.

241 J.-J. Bai, X. Zhang, X. Wei, Y. Wang, C. Du, Z.-J. Wang, M.-L. Chen and J.-H. Wang, *Anal. Chem.*, 2023, **95**(4), 2523–2531.

242 Y. Chen, D. Gao, Q. Zhu, B. Chu, J. Peng, J. Wang, L. Liu and Y. Jiang, *Analyst*, 2023, **148**, 2387–2394.

243 R. Chinnappan, Q. Ramadan and M. Zourob, *Biosens. Bioelectron.*, 2023, **220**, 114856.

244 R. Chinnappan, Q. Ramadan and M. Zourob, *J. Funct. Biomater.*, 2023, **14**(9), 441.

245 L. Zhao, H. Wang, J. Fu, X. Wu, X. Y. Liang, X. Y. Liu, X. Wu, L. L. Cao, Z. Y. Xu and M. Dong, *Biosens. Bioelectron.*, 2022, **214**, 114487.

246 L. Zheng, H. Wang, P. Zuo, Y. Liu, H. Xu and B.-C. Ye, *Anal. Chem.*, 2022, **94**(21), 7703–7712.

247 Z. Zhou, Y. Chen and X. Qian, *Biosensors*, 2022, **12**(4), 257.

248 X. Dong, J. Chi, L. Zheng, B. Ma, Z. Li, S. Wang, C. Zhao and H. Liu, *Lab Chip*, 2019, **19**, 2897–2904.

249 Y. Lu, B. Lin, W. Liu, J. Zhang, L. Zhu, C. Yang and Y. Song, *Small Methods*, 2023, **7**(9), 2300516.

250 G. N. Abdelrasoul, A. Anwar, S. MacKay, M. Tamura, M. A. Shah, D. P. Khasa, R. R. Montgomery, A. I. Ko and J. Chen, *Anal. Chim. Acta*, 2020, **1107**, 135–144.

251 M. Kavruk, Z. Babaie, G. Kibar, B. Çetin, H. Yeşilkaya, Y. Amrani, A. D. Dursun and V. C. Özalp, *Microchim. Acta*, 2024, **191**, 285.

252 W. Liu, C. Zhu, S. Gao, K. Ma, S. Zhang, Q. Du, K. Sui, C. Liu and Z. Chi, *Talanta*, 2024, **266**(Part 2), 125085.

253 Y. Man, M. Ban, A. Li, X. Jin, Y. Du and L. Pan, *Food Chem.*, 2021, **354**, 129578.

254 A. Manfredini, E. Malusà and L. Canfora, *Appl. Microbiol. Biotechnol.*, 2023, **107**, 6963–6972.

255 Y. Suo, W. Yin, Q. Zhu, W. Wu, W. Cao and Y. Mu, *Biosensors*, 2022, **12**(7), 458.

256 Z. Wang, H. Wang, X. Cheng, J. Geng, L. Wang, Q. Dong, C. Liu, Z. Chi and Z. Chi, *Biosens. Bioelectron.*, 2021, **193**, 113551.

257 J. H. Wu, C. H. Wang, Y. D. Ma and G. B. Lee, *Lab Chip*, 2018, **18**, 1633–1640.

258 Z. Zhang, X. Deng, W. Zhang, K. Chen, Y. Su, C. Gao, D. Gong, L. Zhu and J. Cai, *Biomicrofluidics*, 2024, **18**(3), 034104.

259 Z. Zhou, X. Lan, L. Zhu, Y. Zhang, K. Chen, W. Zhang and W. Xu, *J. Hazard. Mater.*, 2023, **445**, 130545.

260 F. Zhu, X. Bian, H. Zhang, Y. Wen, Q. Chen, Y. Yan, L. Li, G. Liu and J. Yan, *Biosens. Bioelectron.*, 2021, **176**, 112943.

261 Z. Zhu, Z. Lv, L. Wang, H. Tan, Y. Xu, S. Li and L. Chen, *Talanta*, 2024, **275**, 126155.

262 D. Raju, S. Bathini, S. Badilescu, A. Ghosh and M. Packirisamy, *Micromachines*, 2022, **13**(5), 730.

263 N. Shaabani, S. R. Meira, M. Marcet-Palacios and M. Kulka, *ACS Pharmacol. Transl. Sci.*, 2023, **6**(3), 387–398.

264 J. C. Contreras-Naranjo, H. J. Wu and V. M. Ugaz, *Lab Chip*, 2017, **17**, 3558–3577.

265 M. J. Alvarez Cubero, J. A. Lorente, I. Robles-Fernandez, A. Rodriguez-Martinez, J. L. Puche and M. J. Serrano, *Methods Mol. Biol.*, 2017, **1634**, 283–303.

266 S. Ju, C. Chen, J. Zhang, L. Xu, X. Zhang, Z. Li, Y. Chen, J. Zhou, F. Ji and L. Wang, *Biomark. Res.*, 2022, **10**, 58.

267 D. D. Dickey and P. H. Giangrande, *Methods*, 2016, **97**, 94–103.

268 G. Attard and J. S. de Bono, *Curr. Opin. Genet. Dev.*, 2011, **21**(1), 50–58.

269 M. M. Ferreira, V. C. Ramani and S. S. Jeffrey, *Mol. Oncol.*, 2016, **10**(3), 374–394.

270 Y. Chen, Y. Yang, J. Feng, A. J. Carrier, D. Tyagi, X. Yu, C. Wang, K. D. Oakes and X. Zhang, *Acta Biomater.*, 2022, **152**, 210–220.

271 R. Gao, C. Zhan, C. Wu, Y. Lu, B. Cao, J. Huang, F. Wang and L. Yu, *Lab Chip*, 2021, **21**, 3888–3898.

272 A. A. Kajani, L. Rafiee, M. Samandari, M. A. Mehrgardi, B. Zarrin and S. H. Javanmard, *RSC Adv.*, 2022, **12**, 32834–32843.

273 M. Li, D. Liu, J. Zhang, X. Zhang and X. Dou, *Anticancer Res.*, 2022, **42**(9), 4345–4358.

274 Y. Liu, Z. Lin, Z. Zheng, Y. Zhang and L. Shui, *ACS Sens.*, 2022, **7**(2), 666–673.

275 J. Dong, G. Li and L. Xia, *Anal. Chem.*, 2022, **94**(48), 16901–16909.

276 S. Khaksari, A. R. Ameri, S. M. Taghdisi, M. Sabet, S. M. J. Ghaani Bami, K. Abnous and S. A. Mousavi Shaegh, *Talanta*, 2023, **252**, 123781.

277 S. Kumamoto, K. Nakatake, S. Fukuyama, K. Yasuda, Y. Kitamura, M. Iwatsuki, H. Baba, T. Ihara, Y. Nakanishi and Y. Nakashima, *Biomicrofluidics*, 2020, **14**(6), 064113.

278 R. Mohammadi, M. Asghari, M. Colombo, Z. Vaezi, D. A. Richards, S. Stavrakis, H. Naderi-Manesh and A. DeMello, *Chimia*, 2022, **76**(No. 7/8), 661–668.

279 N.-V. Nguyen and C.-P. Jen, *Micromachines*, 2019, **10**(3), 195.

280 J. Peng, Y. Liu, R. Su, L. Zeng, Z. Huo, R. Peng, X. Yu, H. Zhang, C. Yang, L. Yang and Z. Zhu, *Anal. Chem.*, 2022, **94**(24), 8766–8773.

281 T. C. Su, H. Vu-Dinh, S. H. Lin, L. Do Quang, T. Chu Duc and C. P. Jen, *Biomed. Microdevices*, 2024, **26**, 7.

282 H. Vu-Dinh, L. Do Quang, C. C. Chang, C. N. Nhu, H. T. Thanh, T. T. Bui, T. C. Duc and C.-P. Jen, *Biomed. Microdevices*, 2021, **23**, 51.

283 H. Vu-Dinh, L. Do Quang, Y. R. Lin and C. P. Jen, *Electrophoresis*, 2023, **44**(11–12), 1002–1015.

284 H. Vu-Dinh, H. Feng and C. P. Jen, *Biosensors*, 2021, **11**(1), 23.

285 C. Wang, Y. Xu, S. Li, Y. Zhou, Q. Qian, Y. Liu and X. Mi, *Mater. Today Bio*, 2022, **16**, 100346.

286 L. Wu, H. Ding, X. Qu, X. Shi, J. Yang, M. Huang, J. Zhang, H. Zhang, J. Song, L. Zhu, Y. Song, Y. Ma and C. Yang, *J. Am. Chem. Soc.*, 2020, **142**(10), 4800–4806.

287 Z. Wu, Y. Pan, Z. Wang, P. Ding, T. Gao, Q. Li, M. Hu, W. Zhu and R. Pei, *J. Mater. Chem. B*, 2021, **9**, 2212–2220.

288 B. Zhang, C. Wang, Y. Du, R. Paxton and X. He, *J. Mater. Chem. B*, 2021, **9**, 7196–7204.

289 X. Zhang, X. Wei, X. Men, C. X. Wu, J. J. Bai, W. T. Li, T. Yang, M. L. Chen and J. H. Wang, *ACS Appl. Mater. Interfaces*, 2021, **13**(36), 43668–43675.

290 R. Siavash Moakhar, R. Mahimkar, A. Khorrami Jahromi, S. S. Mahshid, C. del Real Mata, Y. Lu, F. Vasquez Camargo, B. Dixon, J. Gilleard, A. J Da Silva, M. Ndao and S. Mahshid, *ACS Sens.*, 2023, **8**(6), 2149–2158.

291 X. Fan, Y. Yan, L. Zhao, X. Xu, Y. Dong and W. Sun, *Front. Cell Dev. Biol.*, 2023, **11**, 1183163.

292 N. I. Khan and E. Song, *Micromachines*, 2020, **11**(2), 220.

293 L. Shakeel, A. Khan and A. Akilimali, *Ann. Med. Surg.*, 2024, **86**(5), 2413–2416.

294 M. Kalathingal and Y. M. Rhee, *J. Comput. Chem.*, 2023, **44**(11), 1129–1137.

295 J. E. Rosenberg, R. M. Bambury, E. M. Van Allen, H. A. Drabkin, P. N. Lara Jr., A. L. Harzstark, N. Wagle, R. A. Figlin, G. W. Smith, L. A. Garraway, T. Choueiri, F. Erlandsson and D. A. Laber, *Invest. New Drugs*, 2014, **32**, 178–187.

296 M. Karthikeyan and P. Rathinasabapathi, *Cell. Mol. Bioeng.*, 2024, **17**, 229–241.

297 T. Jalali, M. Salehi-Vaziri, M. H. Pouriayevali and S. L. M. Gargari, *Sci. Rep.*, 2021, **11**, 12639.

298 A. Pourdadashi, R. Rezaei Adriani and S. L. Mousavi Gargari, *J. Biosci. Bioeng.*, 2022, **134**(5), 441–449.

299 M. K. Doherty, C. Shaw, L. Woods and B. C. Weimer, *Microorganisms*, 2023, **11**(7), 1776.

300 O. Uhuo, T. Waryo, M. Oranzie, N. Sanga, Z. Leve, J. January, Z. Tshobeni, K. Pokpas, S. Douman and E. Iwuoha, *Bioelectrochemistry*, 2024, **158**, 108693.

301 D. R. Martin, A. T. Mutombwera, A. M. Madiehe, M. O. Onani, M. Meyer and R. Cloete, *J. Biomol. Struct. Dyn.*, 2024, 1–18, DOI: **10.1080/07391102.2024.2302922**.

302 H. C. Lai, C. H. Wang, T. M. Liou and G. B. Lee, *Lab Chip*, 2014, **14**, 2002–2013.

303 G. Kim, J. Kim, S. M. Kim, T. Kato, J. Yoon, S. Noh, E. Y. Park, C. Park, T. Lee and J.-W. Choi, *Sens. Actuators, B*, 2022, **352**(Part 2), 131060.

304 C. Han, Q. Liu, X. Luo, J. Zhao, Z. Zhang, J. He, F. Ge, W. Ding, Z. Luo, C. Jia and L. Zhang, *Biosens. Bioelectron.*, 2024, **257**, 116313.

305 M. Kołodziej, J. Joniec, M. Bartoszcze, R. Gryko, J. Kocik and J. Knap, *Ann. Agric. Environ. Med.*, 2013, **20**(1), 1–7.

306 G. Park, H. Park, S.-C. Park, M. Jang, J. Yoon, J.-H. Ahn and T. Lee, *Nanomaterials*, 2023, **13**(2), 361.

307 Y. L. Balachandran, X. Li and X. Jiang, *Nano Lett.*, 2021, **21**(3), 1335–1344.

308 H. Rouco, P. García-García, C. Évora, P. Díaz-Rodríguez and A. Delgado, *Int. J. Pharm.*, 2022, **624**, 121973.

309 H. Shan, X. Sun, X. Liu, Q. Sun, Y. He, Z. Chen, Q. Lin, Z. Jiang, X. Chen, Z. Chen and S. Zhao, *Small*, 2023, **19**(7), 2205498.

310 C.-M. Xu, M. Tang, J. Feng, H.-F. Xia, L.-L. Wu, D.-W. Pang, G. Chen and Z.-L. Zhang, *Lab Chip*, 2020, **20**, 1418–1425.

311 K. Yi, Y. Rong, L. Huang, X. Tang, Q. Zhang, W. Wang, J. Wu and F. Wang, *ACS Sens.*, 2021, **6**(4), 1418–1429.

312 S. M. Shea, K. A. Thomas, R. M. G. Rassam, E. P. Mihalko, C. Daniel, B. A. Sullenger, P. C. Spinella and S. M. Nimjee, *Pharmaceuticals*, 2022, **15**(12), 1450.

313 K. Wen, W. Dai, X. Meng, Q. Lin, J. Wei, L. Tong, S. K. Taylor, S. A. Rudchenko, M. N. Stojanovic, G. Kalantarov and I. Trakht, *Biosens. Bioelectron.*, 2024, **246**, 115842.

314 T. N. H. Nguyen, L. F. Horowitz, T. Krilov, E. Lockhart, H. L. Kenerson, T. S. Gujral, R. S. Yeung, N. Arroyo-Currás and A. Folch, *Sci. Adv.*, 2024, **10**(36), eadn5875.

315 Y. Zhu, C. Zou, J. Zhang, W. Jiang, F. Guan, K. Tang, S. Li, G. Li, J. Wang and Z. Ke, *ACS Appl. Mater. Interfaces*, 2020, **12**(5), 5671–5679.